

**UNIVERSITY OF BUCHAREST  
FACULTY OF CHEMISTRY  
DOCTORAL SCHOOL IN CHEMISTRY**

**PhD-THESIS**

**ABSTRACT**

**ACID-BASE MATERIALS FOR GREEN AND SUSTAINABLE  
CHEMICAL PROCESSES**

PhD Student:  
Magdi A. Belkassim EL. Fergani

Supervisor:  
Prof. Dr. Vasile I. Parvulescu

**Doctoral committee:**

President: Prof. Dr. Camelia BALA

Supervisor: Prof. Dr. Vasile I. PARVULESCU

**Official referents:**

1. Prof. Dr. Hermenegildo GARCIA, from Polytechnic University of Valencia, Spain
2. Prof. Dr. Kostas TRIANTAFYLLIDIS, from Aristotle University, Thessaloniki, Greece
3. Prof. Dr. Csaba PAIZS, from Babes-Bolyai University, Cluj-Napoca, Romania

**2021**

## Contents *(corresponding to the PhD thesis)*

|   | Pages |
|---|-------|
| <b>General Introduction</b>   | 8     |
| <b>CHAPTER 1:</b> <i>Biomass-a vast source for the production of biofuels and biochemicals</i>      |       |
| Introduction  | 10    |
| 1.1. Cellulose and cellulose derivatives  | 13    |
| 1.2. Biomass valorization using the biorefinery concept   | 17    |
| 1.2.1. Platform molecules   | 21    |
| 1.2.1.1. Succinic acid (SA)   | 21    |
| 1.2.1.2. Maleic acid (MA)   | 23    |
| 1.2.1.3. Hydroxymethylfurfural(HMF)   | 25    |
| 1.2.1.4. 2,5-furandicarboxylic acid (FDCA)  | 27    |
| References  | 29    |
| <b>CHAPTER 2:</b> <i>Catalysis as a foundational pillar of green chemistry</i>                      |       |
| Introduction  | 36    |
| 2.1. Supported catalysts  | 38    |
| 2.1.1. Zeolites   | 38    |
| 2.1.1.1. Shape-selectivity/acidity and stability of the zeolites                                    | 40    |
| 2.1.2. Magnetic nanoparticles   | 44    |
| 2.1.2.1. Coating of magnetic nanoparticles  | 46    |
| 2.1.3. Valorization of humins as support  | 47    |
| 2.2. Improvement the catalytic properties of the metal oxides                                       | 51    |
| 2.2.1. Acid-base and redox properties of the metal oxides   | 53    |
| 2.2.1.1. Niobium oxides   | 54    |
| 2.2.1.2. Manganese oxides   | 56    |
| 2.2.1.3. Cobalt oxides  | 57    |
| References  | 58    |
| <b>CHAPTER 3:</b> <i>Experimental section: methodologies, instrumentations and common materials</i> |       |
| 3.1. Catalysts preparation  | 68    |
| 3.1.1. Preparation of Nb-zeolite catalysts  | 68    |
| 3.1.1.1 Nb-zeolite catalysts prepared through a two-step  | 68    |

|  |    |
|--|----|
| <i>post synthesis methodology</i>  |    |
| 3.1.1.1.1. Conventional activation protocol: $\text{Na}^+ / \text{H}^+$ ion-exchange       | 68 |
| 3.1.1.1.2. Synthesis of Nb-zeolites through the dealumination of zeolites and Nb insertion | 69 |
| 3.1.1.2. Nb-silicalite catalysts preparation through the sol-gel method                    | 70 |
| 3.1.2. Preparation of the multifunctional magnetic nanocomposites catalysts                | 71 |
| 3.1.2.1. Ru-based $\text{Fe}_3\text{O}_4@ \text{SiO}_2$                                    | 71 |
| 3.1.2.2. $\text{MO}_x\text{-SiO}_2@ \text{Fe}_3\text{O}_4$                                 | 72 |
| 3.1.2.3. $\text{Nb}_2\text{O}_5\text{-SiO}_2@ \text{MNP}$ ( $x\text{Nb}@ \text{MNP}$ )     | 72 |
| 3.1.2.4. $10\text{M}@x\text{Nb}@ \text{MNP}$   | 73 |
| 3.1.3. Niobia supported onto humins  | 74 |
| 3.1.3.1. Humins preparation  | 74 |
| 3.1.3.2. Niobia deposition   | 74 |
| 3.2. Characterization techniques   | 74 |
| 3.2.1. Adsorption-desorption isotherms   | 74 |
| 3.2.2. Powder X-ray diffraction (XRD)  | 75 |
| 3.2.3. Diffuse reflectance spectroscopy with Fourier transforms (DRIFT)                    | 75 |
| 3.2.4. X-ray photoelectron spectroscopy (XPS)  | 75 |
| 3.2.5. Time-of-flight secondary ion mass spectrometry (ToF-SIMS)                           | 76 |
| 3.2.6. Temperature programmed desorption ( $\text{CO}_2/\text{NH}_3$ -TPD)                 | 76 |
| 3.2.7. Scanning electron microscopy (SEM)  | 76 |
| 3.2.8. Dynamic light scattering (DLS)  | 77 |
| 3.2.9. Thermogravimetry-differential thermal analysis (TG-DTA)                             | 77 |
| 3.2.10. Inductively coupled plasma optical emission spectroscopy (ICP-OES)                 | 77 |
| 3.3. Catalytic tests   | 77 |
| 3.3.1. Reaction conditions of Nb-based zeolite catalytic tests                             | 77 |
| 3.3.1.1. Catalytic wet oxidation (CWO) in aqueous phase                                    | 77 |
| 3.3.1.2. Oxidation reactions with organic peroxides  | 78 |
| 3.3.1.3. Products analysis   | 78 |
| 3.3.2. Reaction conditions of multifunctional magnetic nanocomposite catalytic tests       | 79 |
| 3.3.2.1. Catalytic wet oxidation (CWO) in aqueous phase                                    | 79 |

|                   |   |     |
|-------------------|---|-----|
|                   | 3.3.2.2. <i>Oxidation reactions with organic peroxides</i>  | 79  |
|                   | 3.3.2.3. <i>Products analysis</i>   | 80  |
|                   | 3.3.3. Reaction conditions of Nb-based humins catalytic tests   | 80  |
|                   | 3.3.3.1. <i>Products analysis</i>   | 80  |
|                   | References  | 81  |
| <b>CHAPTER 4:</b> | <i>Nb-based zeolites: efficient bi-functional catalysts for the one-pot synthesis of succinic acid from glucose</i>                                       |     |
|                   | Introduction  | 84  |
|                   | 4.1. Objectives   | 84  |
|                   | 4.2. Results and discussion   | 85  |
|                   | 4.2.1. Catalysts characterization   | 85  |
|                   | 4.2.2. Catalytic behavior   | 94  |
|                   | 4.3. Conclusions  | 99  |
|                   | References  | 100 |
| <b>CHAPTER 5:</b> | <i>Optimized Nb-based zeolites as catalysts for the synthesis of succinic acid and FDCA</i>   |     |
|                   | Introduction  | 106 |
|                   | 5.1. Objectives   | 106 |
|                   | 5.2. Results and discussion   | 107 |
|                   | 5.2.1. Catalysts characterization   | 107 |
|                   | 5.2.2. Catalytic behavior   | 115 |
|                   | 5.2.2.1. <i>Catalytic wet oxidation (CWO) in aqueous phase</i>  | 115 |
|                   | 5.2.2.2. <i>Oxidation reactions with organic peroxides</i>  | 119 |
|                   | 5.3. Conclusions  | 121 |
|                   | References  | 122 |
| <b>CHAPTER 6:</b> | <i>Upgrade of 5-hydroxymethylfurfural to dicarboxylic acids onto multifunctional based Fe<sub>3</sub>O<sub>4</sub>@SiO<sub>2</sub> magnetic catalysts</i> |     |
|                   | Introduction  | 129 |
|                   | 6.1. Objectives   | 130 |
|                   | 6.2. Results and discussion   | 131 |
|                   | 6.2.1. The HMF oxidation by noble metal-based catalysts (Ru-based Fe <sub>3</sub> O <sub>4</sub> @SiO <sub>2</sub> )                                      | 131 |
|                   | 6.2.2. HMF oxidation by supported oxide catalysts   | 138 |

|                   |  |     |
|-------------------|--|-----|
|                   | (MnO <sub>x</sub> - and CoO <sub>x</sub> -based Fe <sub>3</sub> O <sub>4</sub> @SiO <sub>2</sub> )           |     |
|                   | 6.3. Conclusions   | 142 |
|                   | References   | 143 |
| <b>CHAPTER 7:</b> | <i>Multifunctional nanocomposites with non-precious metals and magnetic core for 5-HMF oxidation to FDCA</i> |     |
|                   | Introduction   | 150 |
|                   | 7.1. Objectives  | 151 |
|                   | 7.2. Results and discussion  | 151 |
|                   | 7.2.1. Catalysts characterization  | 151 |
|                   | 7.2.2. Catalytic behavior  | 174 |
|                   | 7.3. Conclusions   | 181 |
|                   | References   | 182 |
| <b>CHAPTER 8:</b> | <i>From useless humins by-product to Nb@graphite-like carbon catalysts highly efficient in HMF synthesis</i> |     |
|                   | Introduction   | 189 |
|                   | 8.1. Objectives  | 190 |
|                   | 8.2. Results and discussion  | 190 |
|                   | 8.2.1. Catalysts characterization  | 190 |
|                   | 8.2.2. Catalytic behavior  | 201 |
|                   | 8.3. Conclusion  | 204 |
|                   | References   | 205 |
|                   | <b><i>General Conclusions</i></b>  | 211 |
|                   | <b><i>DISSEMINATION</i></b>  |     |
|                   | I- <i>List of publications relevant for PhD thesis</i>   | 215 |
|                   | II- <i>Miscellaneous publications</i>  | 216 |
|                   | III- <i>Communications</i>   | 216 |

# CHAPTER 1: Biomass-a vast source for the production of biofuels and biochemicals

## Introduction

The dwindling supply of fossil fuels, the disturbing economic impacts of fossil fuel price fluctuations and the threatening effects of climate change have already stimulated an increasing interest and efforts for developing clean and sustainable alternatives

In the new circular economy concept, in addition to the renewable alternative energy resources such as solar, wind and wave power, biomass is considered as the only source that should provide organic carbon as a renewable feedstock to the chemical industry. However, compared to petroleum derived molecules, most biomass-derived ones are highly functionalized (Figure 1). [1].

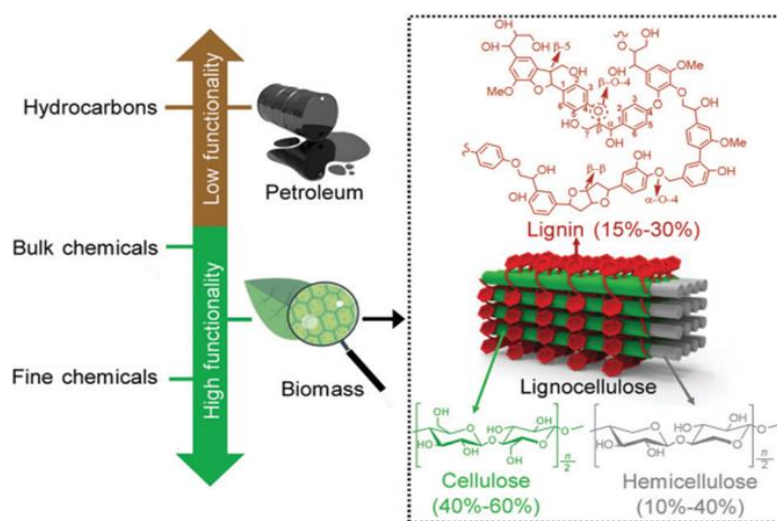


**Figure 1:** Degree of functionality of petroleum, biomass and typical carbon based chemicals. Chemical structures of major components of lignocellulosic biomass, including cellulose, hemicellulose and lignin, are displayed in the right panel.

Therefore, it is mandatory to selectively modify these and for this purpose were recommended depolymerization, hydrolysis, dehydration, deoxygenation, and oxidation. Following these routes biomass can be converted into valuable compounds with new functionalities. Also important, in addition to alleviating the societal dependence on fossil fuel sources, the production of chemicals biomass holds the promise to reduce the production of plastics (ubiquitous in modern life) pollution.

In this context, the conversion of lignocellulosic biomass has become one of the most widely studied routes because of several advantages. Lignocellulose is an inedible and carbon neutral source and its use avoids food vs. fuel issues as for the case of grain and crop based biomass and also important, it is inexpensive.

Lignocellulosic biomass represents more than 90% from the total of biomass. It is a functionalized biopolymer consisting of three major components, i.e., lignin, cellulose and

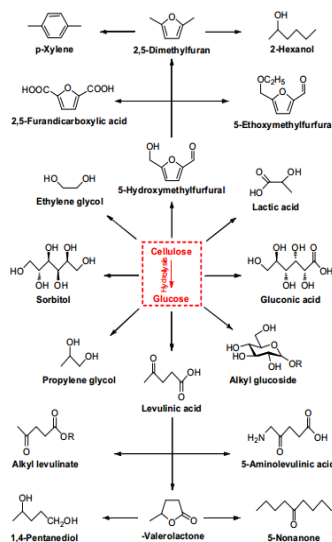
hemicellulose with weight fractions of 15–30%, 40–60% and 10–40%, respectively (Figure 1) [2].

### 1.1. Cellulose and cellulose derivatives

Cellulose is the most abundant component of bio-renewable resources. This relates to both its high natural abundance and well-defined structure consisting of repeating glucopyranose units, linked via  $\beta$ -1,4-glycosidic bonds. Therefore, it was suggested as a strong candidate for the production of several commodities and chemicals such as: textile fibers, bio-fuels, (nano) composites or hydrogels.

Conversion of cellulose into targeted chemicals is considered to be essential for a sustainable development of chemistry. However, it looks less attractive to produce fuels due to the fact the cellulose has a relatively high O/C ratio. This will require a removal of the oxygen that is already not efficient. Therefore, the transformation of cellulose into oxygenates, such as polyols, which is a highly atom-economy process where most of the oxygen-functional groups are preserved, is more attractive [3].

Scheme 1 illustrates several routes considered for the selective transformation of cellulose considering glucose as intermediates. According to Scheme 1, the hydrolysis of cellulose into glucose, as a platform molecule, is a primary and essential step for the transformation of cellulose into chemicals. Glucose is obtained via depolymerization of cellulose under acid catalyzed hydrolysis, which is a versatile precursor to valuable chemicals such as biodegradable plastics and ethanol. The disruption of the  $\beta$ -1,4-glycosidic bonds occurs in the presence of water. However, the formation of glucose parallels its decomposition to several byproducts. The selective production of glucose is even more challenging since in an acidic reaction environment the apparent activation energies of several intermediates are of the same order of magnitude for both decomposition and hydrolysis of cellulose [4].



**Scheme 1:** Selective transformation of cellulose into various chemicals and fuels via glucose as intermediate.

## 1.2. Biomass valorization using the biorefinery concept

The biorefinery concept focuses on the utilization of biomass to generate a range of products as, for example, fuels, platform chemicals and high-value chemicals, using a similar strategy to that has been already utilized in the petroleum refinery. However, since most of the developed processes in the petrochemical industry are not suitable for the conversion of the biomass, alternative pathways for the production of fuels and chemicals are necessary.

Biorefineries can be divided into two categories: (i) the 1<sup>st</sup> generation of biorefinery has been dedicated to edible crops, (ii) the 2<sup>nd</sup> generation focuses to non-edible feedstocks or side streams. Consequently, the 2<sup>nd</sup> generation of biorefinery has a high potential for a sustainable production of energy and chemicals. This approach includes more advanced processes, enabling more value-added products.

Summarizing the achievements to-date, the hemicellulose can be converted to xylose and furfural; cellulose can be hydrolyzed to glucose, HMF, and LA, while xylene, benzene, toluene, and other aromatic compounds can be produced from lignin due to its chemical nature and aromatic structure. The humins are solid residues left from the hydrolysis of biomass. Furfural, glucose, HMF, LA and the other molecule platforms can be further upgraded to biofuels and biofuel additives, while the solid residues can be used to produce energy and aromatic bio-oil.

In conclusion, the development of a sustainable biorefinery is critical to produce high value-added bio-products along with bio-energies in an integrated biorefinery. The production of bio-based chemicals in a biorefinery can significantly reduce the GHG emissions; this would also stimulate an innovative advancement in the area of biorefinery processes and an expand of the biobased economy. Finally it will lead to a more environmentally benign chemical manufacturing industrial sector [5].

### 1.2.1. Platform molecules

Economic and technologic evaluation of the potential products of biorefinery selected a number of compounds that may serve as platform molecules, such as: succinic acid (SA), maleic acid and fumaric acids (MA, FA), 5-hydroxymethylfurfural (HMF) and 2,5-furandicarboxylic acid (FDCA).

In short, it is believed that green, efficient, simple and inexpensive production of these platform molecules from lignocellulose biomass and related downstream products will have broad application prospects and important significance to achieve the future sustainable development of industrial polyester, polyamides, resins....etc, [6].

## CHAPTER 2: Catalysis as a foundational pillar of green chemistry

### Introduction

Acid catalysis demonstrated efficiency for the biomass valorization. For example, following this route, the  $\beta$ -(1,4)-glycosidic bonds of cellulose are cleaved to give glucose, which can be further converted to various organic (bulk) chemicals. Homogeneous catalysts as the mineral acids (such as H<sub>2</sub>SO<sub>4</sub>) were utilized with all the mentioned inconvenience (such as: difficult separation and recovery of the catalysts and limited recycling capability). Also, enzymes were utilized to selectively hydrolyze the cellulose, despite the high costs and small

productivities. Also, the difficulty of recovering the enzyme from the reaction mixtures makes it not industrially suitable.

Working under sub- or supercritical water conditions does not improve the selectivity due to the low thermal stability of the glucose at high temperatures. Higher temperatures and pressures also increase the costs of the production. Based on these reasons, the heterogeneous catalysis remains the only favorable choice offering a sustainable solution to all these problems [7].

## **2.1. Supported catalysts**

In the case of supported particles, the control of the particle size is undoubtedly closely related to the type of the support. Supports with smaller pores and higher surface areas provide a favorable interaction with the particles when smaller NPs are deposited. High surface areas afford a better dispersion of the particles and diminish the leaching when there is a strong affinity with the support. Beside these, the support may exhibit a strong influence on the electronic structure of the supported NPs and/or interfere in the catalytic reaction by itself.

### **2.1.1. Zeolites**

Zeolites are crystalline aluminosilicates with a three-dimensional framework that consists of nanometer-sized channels and cages, affording the high porosity. The three-dimensional framework of zeolites is constructed from corner shared tetrahedral (T-atoms) of silicon and aluminum, bridged via oxygen atoms.

Today there are numerous commercial processes which valorize the properties of zeolites from oil-refining to fine chemicals production through petrochemistry.

Overall, four properties of zeolites make them valuable for heterogeneous catalysis: (1) the preference to exchangeable cations, allowing the introduction of new cations with various catalytic properties; (2) the possibility to induce acidity via exchanging cations with  $H^+$ ; (3) the possibility to tune the pore size; (4) the correlation of the pore diameters with the molecular dimensions of the substrates (i.e., less than 1 nm). Properties 1 and 2 accounts for the catalytic activity while 3 and 4 are responsible for the molecular sieving [8].

Moreover, the synthesis of hierarchical zeolites containing both micropores and mesopores, with strong acidity and high stability, and of mesoporous zeolites allowing an efficient mass transportation extended the use of zeolites in multistep reactions.

Petro-refinery and chemistry require thermally and hydrothermally stable zeolites. In addition, integrated biorefineries involving catalytic biomass transformation steps such as hydrolysis require a catalyst stability in hot liquid water. Unfortunately, most of the zeolites are not stable in such conditions, Al from the zeolite network being leached during such processes. Nevertheless, adapting zeolite properties to the specificity of biomass, mainly aiming at retaining catalytic specificities under conditions of enhanced site accessibility, is not insurmountable. The zeolite dealumination and insertion of a stable cation in hot liquid water offers a solution in this sense. Also, the acidity required for acid catalysis can be induced in zeolites by an isomorphous substitution of the frame-work Al by heteroatoms [9].

### 2.1.2. Magnetic nanoparticles

$\text{Fe}_3\text{O}_4$  NPs have been widely studied as catalysts and catalyst supports for heterogeneous catalysis. A catalyst in nanometer dimensions may afford a substantial enhancement of the catalytic activity. However, another important challenge for the green chemistry is to improve the catalyst separation and its recycling. This aim can be accomplished by using magnetic nanoparticles (MNPs) as a support for the catalytic active phases. Their paramagnetic character allows an easy extraction from the reaction by applying an external magnetic field. Also, they can support various active sites for a multitude of catalytic reactions, especially those carried out in organic solvents (Figure 2) [10].

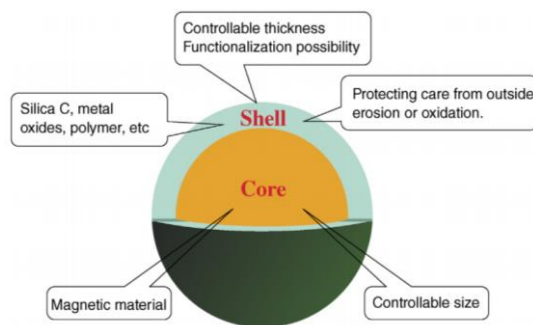


**Figure 2:** Schematic structure of the magnetic core-shell nanoparticles.

### 2.1.3. Valorization of humins as supports

Humins are biomass derived material, and co-products of the acid-catalyzed conversion of carbohydrates, cellulose, and hemicellulose into platform chemicals. Humins are heterogeneous and polydisperse macro-molecules mainly constituted of furanic rings with ketones, aldehydes, and hydroxyls as main functional group.

To improve the economics of the process for commercialization, the coproduction of fuel and chemicals is crucial. The utilization of all biomass derivatives, including cellulose, hemicellulose, and lignin is also mandatory. Thus, it is important to effectively optimize the processes by suppressing the formation of humins and by upgrading these humins byproducts into valuable chemicals or, alternatively, to useful material [11].

The polyaromatic network and abundant oxygen functional groups of humins are intrinsically similar to that of carbohydrate-derived carbonaceous solid acid catalyst, which was first developed by Hara and co-workers [12] by heating various types of carbohydrates (including glucose, starch and microcrystalline cellulose) in inert atmosphere, followed by sulfonation. These results confirm indeed that, it is of great interest to exploit carbonaceous solid acid catalysts by using humins byproduct as precursor and to investigate their structural and catalytic performances. In comparison with the pure carbohydrate-derived carbon, humins-derived carbon is more competitive due to the lower cost; meanwhile, such as application would allow the complete use of feedstock carbon in the biorefinery processes and reduce environmental pollution. So far as we know, there are few reports on the application of humins byproducts as solid acid catalysts.

## 2.2. Improvement of the catalytic properties of the metal oxides

The metal oxides are binary or mixed compounds of elements with oxygen. Most of the metal oxides are ionic network materials. They represent one of the most important and widely employed categories of solid catalysts, either as active phases or supports. In both crystalline and amorphous structures the utilization of these metal oxides in catalysis is related to both the acid–base and redox properties. They constitute a very important family of catalysts in heterogeneous catalysis. Compared to alternative noble metals they have the advantage to be cheap and reliable.

However, the chemistry of the metal oxides is not simple, especially due to the surface contribution. Their manipulation requires a control of the relation between the performance and the fundamental structure–activity relationships [13].

Among the metal oxide catalysts, those of transition metals play a dominant role owing to the relatively low cost of the production, easy regeneration and selective action. These are used in widely different types of organic reactions, such as oxidations, dehydrations, dehydrogenations, isomerizations, and include applications ranging from petrochemical processes to biomass conversion and to the fine chemistry. Supported metal oxides are also used as environmental catalysts to transform selectively undesirable pollutants to nonnoxious forms [14].

The supported catalysts comprise a very general solid catalyst design in which the active phase (the supported layer) is located on the surface of an underlying solid (the support). Obviously, the dispersion and stabilization of the supported layer on a high surface area support lead to a highly active and robust composite catalyst [15].

The major roles of the supports are: (a) to provide a large surface, to separate the active phase and prevent the formation of large crystalline particles; and (b) to supply the space where the catalytic reactions take place.

## CHAPTER 3: Experimental section: methodologies, instrumentations and common materials

### 3.1. Catalysts preparations

All the synthesis reagents were of analytic purity from Sigma-Aldrich and used as received.

#### 3.1.1. Preparation of Nb-zeolite catalysts

##### 3.1.1.1 *Nb-zeolite catalysts prepared through a two-step post synthesis methodology*

##### 3.1.1.1.1 *Conventional activation protocol: Na<sup>+</sup>/H<sup>+</sup> ion-exchange*

Except  $\beta$ -6 zeolite, all other zeolite materials were purchased in the  $\text{NH}_4^+$  form. The ion-exchange protocol was applied only for  $\text{Na}^+$ - $\beta$ -6 zeolite, as following: 100mL of  $\text{NH}_4\text{NO}_3$  0.5 M solution was added to a slurry of 1g of  $\text{Na}^+$ - $\beta$ -6 in water and the mixture was stirred for 12h, at room temperature. After this time, the solid was separated by filtration, washed with deionized water, dried and subjected to a novel treatment with 100 mL of 0.5 M  $\text{NH}_4\text{NO}_3$  solution. The treatment was repeated four times yielding a  $\text{NH}_4^+$ - $\beta$ -6 zeolite. The final solid was separated by filtration, washed with deionized water, and dried under vacuum at 80°C, for 6h.

Finally, the obtained  $\text{NH}_4^+$ - $\beta$ -6 zeolite was calcined in an oven at 450°C, in static air atmosphere, for 10h, when  $\text{NH}_4^+$  was decomposed to  $\text{NH}_3(\text{g})$  and  $\text{H}^+$ , thus generating the  $\text{H}^+$ - $\beta$ -6

zeolite. The calcination temperature was raised with a temperature ramp of 2°C/min. The same calcination protocol was applied to all zeolites. The obtained samples were denoted as H-β-6, H-β-12, H-β-18, H-β-37, H-ZSM25, H-Y5 and H-Y30.

### ***3.1.1.1.2. Synthesis of Nb-zeolites through the dealumination of zeolites and Nb insertion***

Nb-β zeolites (1.6 wt % Nb, 0.02 mol %) were prepared through a two-step post-synthesis protocol. Accordingly, the siliceous (dealuminated) β zeolites were prepared by treating the NH<sub>4</sub><sup>+</sup>-β zeolite materials (Si/Al = 6, 12, 18 and 37.5) with nitric acid as follow: 2.3 g NH<sub>4</sub><sup>+</sup>-β zeolite was poured in a solution of (0.25N) HNO<sub>3</sub> and the mixture was stirred at 80°C, for 4h. In parallel, part of NH<sub>4</sub><sup>+</sup>-β (i.e. 2.5g) was treated with 50 mL of 0.1N oxalic acid solution. The suspension was then kept at room temperature for 8 h. After the separation, the samples were washed with deionized water and dried overnight in an oven at 120°C. The obtained sample was denoted as De-Al-β. Then, 2g of De-Al-β were poured in 100 mL of an isopropanol solution containing 3.5×10<sup>-3</sup> mol.L<sup>-1</sup> niobium ethoxide (Nb(OC<sub>2</sub>H<sub>5</sub>)<sub>5</sub>) and stirred for 3h, at 80°C, under inert atmosphere. After that the mixture (pH=5.6) was stirred at 80°C, for 1h, in air, until a complete removal of isopropanol. The resulted solid was washed three times with distilled water, dried in air at 80°C for 24h, and calcined at 450°C in a static air atmosphere for 10h.

Following a similar protocol, similar samples with a final concentration of 0.05 mol% Nb were prepared by adjusting the amount of raw material.

A similar protocol was applied for the other zeolites and obtained catalysts, were denoted as: Nb-ZSM25, Nb-Y5 and Nb-Y30, where the number represents the Si/Al ratio.

### ***3.1.1.2. Nb-Silicalite catalysts preparation through the sol-gel method***

The synthesis of NbSi-1 followed a reported procedure [16]. In agreement with this procedure, 10.8 mL of tetrabutylammonium hydroxide solution ((TBA)OH) was slowly added to 14.2 g of tetraethyl orthosilicate (TEOS) under stirring. In parallel, 1.7 mL of niobium ethoxide (corresponding to a final concentration of Nb of 0.05%mol) was slowly added to 10 mL of dry ethylic alcohol while stirring. The two solutions were then mixed by adding dropwise the niobium ethoxide solution to the TEOS-(TBA)OH solution, and the obtained mixture was stirred for 15 min. To this mixture, another 4.0 mL of aqueous (TBA)OH solution was slowly added. The final solution was heated to 70°C under stirring, while water was added to compensate for the loss due to the evaporation. The formed gel (60 mL) was then transferred into an autoclave and heated to 170°C for 40 h without stirring. After crystallization, the product was separated from the mother liquor, washed with distilled water, and dried at 80°C overnight. In the final step, the synthesized samples were calcined at 550°C in air, for 20 h, to remove the organic template.

Silicalite-1 sample was also prepared by applying a similar method as above except that the step for the addition of Nb was omitted. The obtained samples were designated as Si-1 and Nb-Si-1.

### **3.1.2. Preparation of the multifunctional magnetic nanocomposites catalysts**

The multi-functional magnetic nanocomposites were prepared by covering nano-magnetic cores (MNP) with two types of mesoporous shells, SiO<sub>2</sub> and Nb<sub>2</sub>O<sub>5</sub>-SiO<sub>2</sub> (denoted as:

$\text{Fe}_3\text{O}_4@\text{SiO}_2$  and  $x\text{Nb}@MNP$ , where  $x$  represents the Si/Nb ratio) followed by  $\text{CoO}_x$ ,  $\text{MnO}_x$  or  $\text{FeO}_x$  (10 wt%) deposition by impregnation-precipitation.

### **3.1.2.1. Ru-based $\text{Fe}_3\text{O}_4@\text{SiO}_2$**

The preparation of a multifunctional Ru-based ( $\text{Fe}_3\text{O}_4@\text{SiO}_2$ ) magnetic catalyst was carried out following previous reported procedures [17]. Briefly, the synthesis of Ru (4wt%)- $\text{Fe}_3\text{O}_4@\text{SiO}_2$  was carried out in three steps: i) 10 mL  $\text{NH}_3\text{OH}$  (25%) and 3.5 mL of TEOS were added to magnetic particles dispersed into ethanol and the mixture was stirred overnight at 40°C. Then, the coated particles were washed with water and ethanol and dried for 24h, at 80°C; ii) the resulted coated particles were then subjected to silanization with (3-aminopropyl) triethoxysilane (APTES) as follows: 3 g of silica coated magnetic particles were suspended in 80 mL 10% (v/v) APTES aqueous solution in a round-bottom flask. After that, 40 mL of glycerol were added and the solution was stirred at 90°C under inert atmosphere for 5 h. After the magnetic separation, the silanized magnetite particles were washed with distilled water and methanol and dried, yielding a fine powder; iii) the APTES silica coated magnetic nanoparticles were impregnated with an aqueous  $\text{RuCl}_3$  solution at basic pH (pH=13) as follows: 1.5 g  $\text{Fe}_3\text{O}_4\text{-SiO}_2/\text{NH}_2$  were added to 200 mg  $\text{RuCl}_3$  aqueous ruthenium (III) chloride (Aldrich) dissolved in 400 mL distilled water. The pH was adjusted at 13 with the aid of a  $\text{NaOH}$  aqueous solution (1M). Then, the mixture was stirred at 25°C for another 24 h. The resulted solid was magnetically collected from the solution, washed twice with distilled water and acetone and dried under vacuum. The same procedure was applied for the synthesis of Ru(3wt%)-  $\text{Fe}_3\text{O}_4@\text{SiO}_2$  catalyst, by adjusting the amount of  $\text{RuCl}_3$  aqueous precursor in step iii).

### **3.1.2.2. $\text{MO}_x\text{-SiO}_2@ \text{Fe}_3\text{O}_4$**

$\text{SiO}_2@ \text{Fe}_3\text{O}_4$  was first synthesized as follow: 10 mL  $\text{NH}_3\text{OH}$  (25%) and 3.5 mL of TEOS were added to magnetic particles dispersed into ethanol and the mixture was stirred overnight at 40°C. Then, the coated particles were washed with water and ethanol and dried for 24h, at 80°C.

$\text{Fe}_3\text{O}_4@\text{SiO}_2\text{-MnO}_x$  and  $\text{Fe}_3\text{O}_4@\text{SiO}_2\text{-CoO}_x$  with 1, 5 and 10wt% of  $\text{MnO}_x$  or  $\text{CoO}_x$ , respectively, were prepared from a M(II) acetate (M = Mn or Co) precursor as follow: the corresponding amount of M(II) acetate was dissolved in 10 mL of distilled water.  $\text{Fe}_3\text{O}_4@\text{SiO}_2$  particles were added to this solution under stirring and after 5 min an aqueous solution of  $\text{NaOH}$  (1M) was drop-wise added until a pH of 10.5 and the mixture was heated at 60°C for 4h. After filtration, the solid was washed with distilled water until neutral pH, then dried in air at 80°C for 24h, and under vacuum at 110°C for 6h, and finally calcined in static air at 500°C (heating rate 1°C/min) for 3h.

### **3.1.2.3. $\text{Nb}_2\text{O}_5\text{-SiO}_2@MNP$ ( $x\text{Nb}@MNP$ )**

The Nb incorporation inside the pore walls was carried out through the Atrane method, versatile in developing mesoporous materials with uniform and high dispersed heteroelements in the silica hydrophilic matrix [18]. Water needed for TEOS hydrolysis was added simultaneously with the corresponding amount of MNPs in order to ensure an uniform packaging with the mesoporous  $\text{Nb}_2\text{O}_5\text{-SiO}_2$  shell. In this way stable links between the -OH groups existing on the

MNPs surface and those generated by TEOS hydrolysis were obtained. For the synthesis of the 22Nb@MNP (Si/Nb = 22) sample the molar ratio of reagents in the native solution was adjusted to  $2-x\text{Si}:x\text{Nb}:7\text{TEAH}_3:0.5\text{NaOH}:0.52\text{CTAB}:180\text{H}_2\text{O}$ , where  $x = 0.087$ , at a pH of 11. The following methodology was used: 0.5 g (0.0125 mol) of NaOH was dissolved in 23 mL (0.172 mol) tri-ethanolamine (TEAH<sub>3</sub>) at 60°C. Immediately, 10.54 mL (0.046 moles) of tetraethyl ortho-silicate (TEOS) and 0.544 mL (0.002 moles) of Nb(OEt)<sub>5</sub> were added and the obtained mixture was stirred at 130°C for 5 min. Then the temperature was reduced at 110°C and 4.68 g (0.013 moles) cetyl-trimethyl-ammonium bromide (CTAB) were added under stirring. After a further adjusting of the temperature at 60°C, 80 mL (4.44 moles) of water and 0.5 g of MNP were added and, in a very short time, a white suspension was formed. This was left to ripen at room temperature, for 24 hours. The resulted solid was filtered, washed with water and ethanol and dried in air. Finally, to release the mesoporous system, the surfactant (CTAB) was extracted from the solid with a solution of acetic acid/ethyl alcohol. For this, approximately 1 g of solid was suspended in a solution of 8 mL CH<sub>3</sub>COOH (80%) and 120 mL ethyl alcohol (99%), and the obtained mixture was refluxed at 60°C for 2 h. To complete the extraction process, the suspension was refluxed at 60°C for another 16h, with a new mixture of CH<sub>3</sub>COOH/ethyl alcohol. The obtained material was collected by filtration, washed with ethanol and dried at 80°C for 24h and then dried under vacuum at 110°C for 6h. Part of the samples was calcined in a static atmosphere, at 500°C for 3h. In a similar way a sample with a Si/Nb ratio of 50 was synthesized by adjusting the amounts of TEOS and Nb(OEt)<sub>5</sub> ( $x = 0.039$ ). These samples were denoted xNb@MNP, where x represents the Si/Nb ratio of 22 and 50, respectively.

#### **3.1.2.4. 10M@xNb@MNP**

To an aqueous solution of M(II) acetate (where: M(II) = Co, Mn or Fe), obtained by dissolving the salt in 10 mL of water, at room temperature, the xNb@MNP was added under strong stirring. After 5 min, an aqueous solution of NaOH (1M) was added drop-wise till pH = 10.5 and the obtained mixture stirred for 4h at 60°C. After reaction the solid was separated by filtration, washed till neutral pH, dried in air, at 80 °C, for 24h, then under vacuum at 110°C, for 6h and calcined in static atmosphere, at 500 °C for 3h. The final samples were denoted as: 10M@xNb@MNP, where: M = Co, Mn or Fe and x = Si/Nb ratio of 22 or 50. Theoretical loadings of Nb were 0.825 wt% (0.01 mol%) for the catalysts with a Si/Nb ratio of 50, and 1.82 wt% (0.02 mol%) for the catalysts with a Si/Nb ratio of 22. The loading of MO<sub>x</sub> (*i.e.*, CoO<sub>x</sub>, MnO<sub>x</sub> or FeO<sub>x</sub>) was 10 wt%, irrespective of the Si/Nb ratio.

### **3.1.3. Niobia-supported humins**

#### **3.1.3.1. Humin preparation**

Humins were prepared from an aqueous solution containing D-glucose (1.0M) and H<sub>2</sub>SO<sub>4</sub> (0.01M) by heating it at 200°C in autoclave, for 12h. Obtained humins were isolated by filtration, washed with water (3 L), dried for 12 h at 80°C, and grounded. After Soxhlet extraction with water for 24 h three times, the samples were dried for 24 h, at 80°C. Following the described preparation conditions, humins were obtained with an yield of 30%. Obtained humin was abbreviated GH.

### 3.1.3.2. Niobium deposition

Catalysts with 1.2 (0.03mol%, 2.5wt%) (GHNb1.2) and 1.7 mmols Nb (0.04mol%, 3.5wt%) (GHNb1.7) were prepared by a deposition precipitation-carbonization (DPC) method as following: urea ( $\text{CON}_2\text{H}_4$ , 0.3g) and ammonium niobate(V) oxalate hydrate ( $\text{C}_4\text{H}_4\text{NNbO}_9\text{xH}_2\text{O}$ , 0.36 or 0.51 g) were added to a slurry of 4.0 g of humins in 250 mL dionized water. The mixture was heated in an autoclave at  $200^\circ\text{C}$  for 12 h. The separated solid was then pyrolyzed at  $450^\circ\text{C}$ , for 4 h, in a  $\text{N}_2$  flow of  $30\text{ cm}^3\text{ min}^{-1}$ .

## 3.2. Characterization techniques

The prepared catalysts were exhaustively characterized using different techniques, such as: BET,  $\text{CO}_2/\text{NH}_3$ -TPD measurements, XRD, XPS, SEM-EDX, ToF-SIMS, ICP-OES, DLS, TG-DTA and DRIFT spectroscopy.

## 3.3. Catalytic tests

### 3.3.1. Reaction conditions of Nb-based zeolite catalytic tests

#### 3.3.1.1. Catalytic wet oxidation (CWO) in aqueous phase

The activity tests in batch mode were carried out in a steel autoclave by adding 0.03-0.05 g of Nb-based zeolite catalyst to a solution of 0.5 mmoles of HMF in 10 mL of water. After closing, the reactor was pressured at 1–18 bars with molecular oxygen (purity  $\geq 99.999\%$  (v/v); Linde 5.0) and heated up to  $80$ – $180^\circ\text{C}$ , under stirring (1200 rpm), for 2–24 h. Parallel tests in the presence of glucose (0.5mmoles) were also performed. After reaction, the oxygen was released, the catalyst was recovered by centrifugation, and the products separated by distillation under vacuum.

#### 3.3.1.2. Oxidation reactions with organic peroxides

Catalytic experiments were performed under vigorous stirring in a stainless steel autoclave (15 mL, HEL Instruments) under the following conditions: 50 mg HMF, 4.4 mL acetonitrile (ACN), 0.18 mL t-BuOOH (solution of 70%) and 25 mg catalyst were stirred at  $120$ – $140^\circ\text{C}$ , for 12–48 h. After reaction, the catalyst was recovered by centrifugation and the products separated by distillation under vacuum.

### 3.3.2. Reaction Conditions of multifunctional magnetic nanocomposite catalytic tests

#### 3.3.2.1. Catalytic wet oxidation (CWO) in aqueous phase

Catalytic experiments were performed in a stainless steel autoclave (15 mL, HEL Instruments) under the following conditions: 50 mg of HMF (i.e., 0.4 mmol), 5 mL of distilled water and 25 mg of catalyst were stirred, at  $110$ – $180^\circ\text{C}$ , under 10–18 atm of molecular oxygen (purity  $\geq 99.999\%$  (v/v); Linde 5.0) for 2–24 h. Parallel tests in the presence of n-butylamine and NaOH were also performed with or without catalyst. Before running the experiments, the reactor was sealed and purged three times with oxygen to remove the residual air. After reaction, the catalyst was magnetically recovered by placing a permanent magnet on the reactor wall and the products were separated by distillation under vacuum.

### **3.3.2.2. Oxidation reactions with organic peroxides**

Catalytic experiments were performed under a vigorous stirring in a stainless steel autoclave (15 mL, HEL Instruments) under the following conditions: 25 mg HMF, 4.4 mL solvent (i.e., acetonitrile (ACN), water or water:methanol (50:50 v/v) mixture), oxidation agent (t-BuOOH (0.18mL, 70 wt% in water), H<sub>2</sub>O<sub>2</sub> (0.16 mL, 30 wt%) and 25 mg catalyst (i.e., MO<sub>x</sub>-SiO<sub>2</sub>@MNP, xNb@MNP and 10M@xNb@MNP). The catalytic experiments were carried out under autogenic pressure, at 80–100°C for 2–24 h. After reaction the reactor was cooled at room temperature, the catalyst was magnetically recovered by placing a permanent magnet on the reactor wall and the products were separated by distillation under vacuum.

### **3.3.2.3. Products analysis**

The recovered products were silylated, diluted with 1 mL of toluene and analyzed by GC-FID chromatography (GC-Shimadzu apparatus). The identification of the products was made using a GC-MS (Carlo Erba Instruments QMD 1000) equipped with a Factor Four VF-5HT column.

### **3.3.3. Reaction conditions of Nb-based humins catalytic tests**

The activity tests in the batch mode were carried out as follows: 0.05g of catalyst was added to a solution of 0.18 g (1.0 mmole) glucose in 5 mL water. After closing, the reactor was heated up to 160-180°C, under stirring (1000 rpm), for 6-12 h. Additional catalytic tests were made in the same conditions but in a biphasic solvent formed from 3.5 mL aqueous solution of 20% NaCl and 1.5 mL organic solvent. As organic solvent 2-sec-butylphenol (SBP), 2-tert-butylphenol (TBP) and methyl isobutyl ketone (MIBK) were used.

For recycling tests, the recovered catalyst was washed with distilled water and centrifuged three times, then dried at 80°C and calcined at 400°C in N<sub>2</sub> flow for 4h.

#### **3.3.3.1. Products analysis**

After reaction, the catalyst was separated by centrifugation and the reaction products were analyzed in both phases by HPLC chromatography, in following conditions: mobile phase: acetonitrile/water = 75/25; flow rate: 1 mL/min; detectors: diode-array detection (DAD), at 254 and 210 nm, and differential refractometer (RID); column: Zorbax Carbohydrate, 4.6x250 mm, 5 micron. Retention times: HMF: DAD, 254 nm: 2.86 min; RID: 3.09 min; levulinic acid: DAD, 210 nm: 7.6 min; RID: 7.9 min; fructose: DAD, 210 nm: 8.4 min; RID: 8.9 min; glucose: RID: 9.7 min, 10.1 min and 10.4 min.

## **CHAPTER 4: Nb-based zeolites: efficient bi-functional catalysts for the one-pot synthesis of succinic acid from glucose**

In this work we focused on a post synthesis strategy for the production of highly dispersed Nb species (0.02-0.05 moles%) into the BEA-zeolite matrix. This strategy supposes a successive zeolite dealumination followed by its impregnation with Nb ethoxide. The new catalysts

demonstrated a high catalytic efficiency for the direct synthesis of succinic acid (SA) from glucose and a very good stability against water.

As strategy, the catalytic wet oxidation (CWO) of glucose was applied. In the absence of a catalyst, WO of glucose is a very unselective process [17] but, in the presence of a catalyst CWO can provide, in principle, a very appealing green route for the synthesis of platform molecules usable for the monomers production. Indeed, the reactions carried out with Nb-based zeolite catalysts in water, as solvent, and molecular oxygen, as solely oxidation reagent, afforded the direct oxidation of glucose to SA.

The catalytic performances, expressed in terms of SA yields, were directly correlated to the nature of the catalytic sites which, in turn, has been dictated by the niobia content and the preparation route.

Lower loadings of niobium (i.e., 0.02 mol%) and temperatures below (i.e., 180°C) led to lower selectivities to succinic acid (Table 1). Interesting enough, the selectivity to succinic acid is favored by the presence of catalysts with higher Si/Al ratios. In accordance, the highest selectivity to SA (83.6%), for a total conversion of glucose, was obtained in the presence of Nb(0.05)- $\beta$ -37.5, dealuminated with nitric acid (Table 1).

The corresponding Nb(0.05)- $\beta$ -37.5O sample, produced in the presence of oxalic acid, led to a selectivity of succinic acid of only 70% for a total conversion of glucose.

**Table 1:** Reaction products distribution in CWO tests

| Entry | Catalyst                | X, % | S, % |     |      |      |
|-------|-------------------------|------|------|-----|------|------|
|       |                         |      | LA   | GA  | LevA | SA   |
| 1     | Nb(0.02)- $\beta$ 12    | 86.2 | 3.1  | 5.9 | 19.0 | 52.0 |
| 2     | Nb(0.05)- $\beta$ 12    | 100  | 1.0  | 3.1 | 5.3  | 62.3 |
| 3     | Nb(0.05)- $\beta$ 18    | 100  | 3.1  | 2.1 | 16.6 | 72.3 |
| 4     | Nb(0.05)- $\beta$ 37.5  | 100  | 0.6  | 0.9 | 3.5  | 83.6 |
| 5*    | Nb(0.05)- $\beta$ 37.5  | 98.7 | 2.8  | 4.3 | 22.7 | 58.3 |
| 6     | Nb(0.05)- $\beta$ 37.5O | 100  | 0    | 1.3 | 10.2 | 70.1 |

**Reaction conditions:** 90 mg glucose; 50 mg catalyst; 10 mL water; 18 bar O<sub>2</sub>, 180 °C, 12 h; \* - 160 °C;  
LA- lactic acid; GA – glycolic acid, LevA – levulinic acid; SA – succinic acid

It is likely that lactic and glycolic acids are formed via the already proposed mechanism of the glucose degradation [19]. On bifunctional catalysts, levulinic acid can also be produced from glucose, usually in two steps involving the glucose isomerisation to fructose on Lewis acid centers followed by the fructose dehydration to LevA through a HMF intermediate on Brønsted acid centers [20]. However, the dehydration of glucose to levulinic acid through a levoglucosane intermediate is also possible on materials presenting exclusively Brønsted acidity [21]. In the absence of oxygen, at 180°C with Nb(0.05)- $\beta$ -18 as catalyst, glucose is dehydrated to HMF (5-hydroxymethylfurfural) and levulinic acid with selectivities of 22.0% and 8.0%, respectively. However, comparing with the CWO reaction, in the presence of the same catalyst and under 18 atm O<sub>2</sub> (Table 1, entry 3) the dehydration of glucose takes place with a much lower conversion (47.4%) and after 24 h.

Unfortunately, during the glucose dehydration, besides HMF and levulinic acid, a large spectrum of other water soluble side products and unwanted HMF aldol-condensation by-products, generically called "humins", are obtained in high amounts. These humins block the active sites of the catalysts, leading to lower catalytic performances. The presence of molecular

oxygen seems to be beneficial in avoiding the formation of such unwanted products (i.e., *humins*). In addition, for all CWO reactions the conversion of glucose is faster and orientated to the targeted reaction product, namely, succinic acid.

## Conclusions

Inserting Nb into the Beta zeolite framework does not replace the aluminum from the tetrahedral spaces. A post-synthesis methodology, however, offers a very high dispersion of the linked Nb(V) species. In accordance to the characterization results, the most probable state of Nb(V) corresponds to Nb(V)O-H where niobium is linked through Nb-O-Si bonds to the zeolitic walls. The tetrahedrally coordinated Al is extracted from the zeolite framework during the preparation process, and deposited mainly as Al-O extra-framework species on the zeolite surface. These residual extra-framework aluminum species exhibit a stronger acidity and also prevent the solubilization of the zeolite framework in hot water. Accordingly, bi-functional materials were produced after the post-synthetic insertion of Nb in the zeolite matrix.

These new catalysts have shown a high efficiency for one-pot oxidizing glucose to succinic acid. The extra-framework aluminum species most likely dehydrate glucose to levulinic acid (LA), which is in turn efficiently oxidized by the Nb species to succinic acid (SA).

These novel catalysts can serve as an alternative to the already reported catalysts based on the Ru critical element. In the presence of Nb(0.05)- $\beta$ -37.5 catalyst, succinic acid is produced in water with a selectivity of 84%, for a total conversion of glucose, after 12h, at 180°C and 18 bar of oxygen.

## CHAPTER 5: Optimized Nb-based zeolites as catalysts for the synthesis of succinic acid and FDCA

Taking as a reference the reported results using Nb-based BEA zeolite catalysts (*Chapter 4*) for the glucose oxidation and with the aim to extend the Nb-based zeolites catalysts applicability, in this work we focused our efforts on the optimization of the catalyst design. Several zeolites (e.g., Y, USY and ZSM-5) with different Si/Al ratios and textural characteristics were considered as carriers for niobium (0.05 mol%) following a Nb post-synthesis methodology. With the same goal, Nb-based Silicalite-1 was prepared *via* a direct synthesis procedure. Data collected from different characterization techniques allowed us to correlate the catalytic efficiency - catalytic properties and, based on this, to establish the main catalytic features of the developed materials able to lead to an optimum catalytic system for the oxidation of glucose and HMF toward SA and HMF toward FDCA.

As Table 2 shows, all samples display both acid and basic sites. While the acidity can be generated by different species such as residual Al framework and extra-framework  $AlO_x(OH)$  species, framework SiO-H groups, extra-framework isolated Nb(V)O-H and  $Nb_2O_5$  pore-encapsulated clusters, the only sites which may display a base character rather than an acidic one are the Nb-OH ones, as also suggested by several authors for niobia-silica mixtures [22]. The total basicity decreased in the following order: Nb-ZSM25 > Nb-Y5 > Nb-Y30 > Nb-Si-1 while the highest concentration of acid sites was measured for Nb-Y5 sample. Interesting enough, for Nb-Si-1, the strength of basic sites is higher compared to other Nb-containing zeolites. The relative high desorption temperature of ammonia for the same catalyst can be correlated to the

strength of niobium acid species (i.e., Nb=O or/and NbO-H). Finally, the base/acid sites ratio decrease in the order Nb-Si-1 > Nb-ZSM25 > Nb-Y30 > Nb-Y5.

**Table 2:** Acid-base sites concentration determined through NH<sub>3</sub>- and CO<sub>2</sub>-TPD

| Sample   | Acid sites concentration<br>(mmols NH <sub>3</sub> /g catalyst) | Base sites concentration (mmols CO <sub>2</sub> /g catalyst) |           |       | Base/acid ratio |
|----------|---|--|-----------|-------|-----------------|
|          |   | 100-170°C  | 190-250°C | Total |                 |
| Nb-Y5    | 0.235 (133°C)   | 0.046  | 0.001     | 0.047 | 0.20            |
| Nb-Y30   | 0.085 (99°C)  | 0.035  | 0.003     | 0.038 | 0.45            |
| Nb-ZSM25 | 0.043 (116°C)   | 0.070  | -         | 0.070 | 1.63            |
| Nb-Si-1  | 0.016 (135°C)   | 0.001  | 0.026     | 0.027 | 1.69            |

Overall, the characterization results are in line with those previously reported (*Chapter IV*) showing that a post-synthetic insertion of Nb in the zeolite matrix led to Nb-zeolite catalysts comprising of extra-framework isolated Nb(V) sites (corresponding to Nb(V)O-H species) and Nb<sub>2</sub>O<sub>5</sub> pore-encapsulated clusters. Also important, they were also detected residual framework Al-acid sites with a strong acidity, which prevent the solubilization of the zeolite framework in hot water [23]. As a function of the Si/Al ratio, the dealumination process takes place in different degrees, generating acid sites with different strength and structures with monomodal mesoporosity. The direct synthesis procedure applied for the preparation of the Nb-Si-1 sample led to tetrahedral species presenting a -Nb=O group and bimodal micro-mesoporosity, also in concordance to literature reports [22]. The presence of niobium species generates both extra acid and basic sites.

The CWO of glucose leads to higher selectivities in SA than HMF, irrespective of the catalyst nature but its magnitude is highly influenced by the base/acid site ratio in the catalyst (Figure 3).

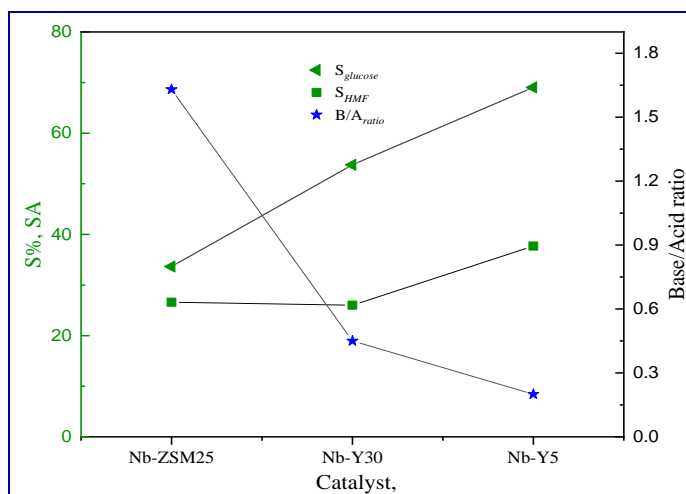


**Figure 3:** The variation of the SA selectivities as a function of the catalyst nature and the base/acid ratio

The failure of the above attempts for the production of FDCA from HMF made us to move from the WO conditions to a catalytic oxygen transfer methodology, which requires oxygen donors such as H<sub>2</sub>O<sub>2</sub> or RO<sub>2</sub>H.

Based on this, all reactions were made by using *t*-butyl hydroperoxyde (*t*-BOOH) as an oxygen transfer agent and the main obtained results are presented in Table 3.

As Table 3 shows, under the investigated reaction conditions Nb-zeolite based catalysts displayed from moderate (53-54%) to high (99.0%) HMF conversio

**Table 3:** The oxidation of HMF with *t*-butyl hydroperoxyde (*t*-BOOH) and in the presence of Nb-based zeolites catalysts

| Entry | Catalyst | Reaction time, h | X, % | S <sub>HMFCA</sub> , % | S <sub>DFF</sub> , % | S <sub>FDCA</sub> , % |
|-------|----------|------------------|------|------------------------|----------------------|-----------------------|
| 1     | Nb-BEA18 | 24               | 53.9 | 73.8                   | 0                    | 5.6                   |
| 2     | Nb-Y30   | 12               | 85.8 | 22.3                   | 0                    | 8.1                   |
| 3     |          | 24               | 99.1 | 41.7                   | 0.6                  | 22.5                  |
| 4     | Nb-Y5    | 12               | 80.5 | 52.1                   | 0                    | 21.4                  |
| 5     |          | 24               | 71.0 | 53.1                   | 0                    | 23.1                  |
| 6     | Nb-ZSM25 | 12               | 53.3 | 73.2                   | 1.2                  | 12.6                  |
| 7     |          | 24               | 96.7 | 15.0                   | 0                    | 61.3                  |
| 8     | Nb-Si-1  | 12               | 95.0 | 47.3                   | 0.6                  | 15.2                  |
| 9     |          | 24               | 99.0 | 47.0                   | 0                    | 26.0                  |
| 10    |          | 48               | 99.0 | 9.2                    | 0                    | 63.8                  |

**Reaction conditions:** 0.050 g HMF, 0.025 g catalyst, 4.4 ml acetonitrile, 0.18 ml 70% *t*-BuOOH, 140 °C, 1000 rpm. Note: the difference in selectivity till 100 is given by lactic, glycolic and succinic acid.

After 12h the FDCA selectivity was less than 20%, irrespective of the catalyst nature. The best catalytic results were obtained after 24-48h, in the presence of Nb-ZSM25 (61.3% FDCA selectivity for a HFM conversion of 96.7%) and Nb-Si-1 (63.8% FDCA selectivity for a HFM conversion of 99.0%) catalysts. Interesting enough, the DFF intermediate was identified only aleatory and in very low amounts. Accordingly, the reasonable reaction pathway for the HMF oxidation over these catalysts should follow the HMF → HMFCa → FFCA → FDCA sequence that is similar with that for supported Au and Pd catalysts [24] and for recently reported 10M@xNb@MNP (where M = Co, Mn and Fe) catalysts [25]. This route indicates a preferential adsorption of -CHO side chain of HMF, which requires the presence of basic sites and positive surface of the catalyst [26]. Differently to BEA and Y zeolites based catalysts, such conditions are properly supplied by Nb-ZSM25 and Nb-Si-1 which was characterized by the presence of both basic and acid sites at temperature the reaction is carried out (see the CO<sub>2</sub>- and NH<sub>3</sub>-TPD analysis results). Among the investigated catalysts these displayed the highest base/acid sites ratio, with a domination of the basic sites (Table 2). These high basic OH<sup>-</sup> ions catalyze the formation of geminal diols from aldehyde and water, while the Nb<sup>+</sup> species catalyze the dehydrogenation steps, in accordance to a mechanism proposed by Donoeva et al [26] for the HMF oxidation on gold nanoparticles supported on basic carbon materials and recently confirmed in our group for 10M@xNb@MNP (where M = Co, Mn and Fe) catalysts [25].

## Conclusions

In summary, Nb-zeolites based catalysts afford highly efficient catalytic systems for the oxidation of glucose and HMF to succinic acid or the oxidation of HMF to FDCA.

The characterization results showed that through the post-synthetic insertion of Nb in the zeolite matrix, the resulted Nb-zeolite catalysts possess a mono-modal mesoporous texture that comprises extra-framework isolated Nb(V) sites (corresponding to Nb(V)O-H species) and Nb<sub>2</sub>O<sub>5</sub> pore-encapsulated clusters. Residual framework Al-acid sites are also formed, which

prevent the solubilization of the zeolite framework in hot water, but also different amounts of extra framework  $\text{AlO}_x(\text{OH})$  species. However, the geometry of Nb is clearly dependent on the synthesis method. Accordingly, while dealumination followed by Nb insertion (i.e., Nb-Y5, Nb-ZSM25, Nb-Y30, Nb-BEA12 and Nb-BEA18) led to the above niobium species, the direct synthesis procedure (i.e., Nb-Sil-1) led to a bi-modal micro-mesoporous structure with tetrahedral niobium species presenting  $-\text{Nb}=\text{O}$  group.

$\text{CO}_2$ - and  $\text{NH}_3$ -TPD measurements evidenced the presence of both acid and basic sites. The only sites which may display a base character rather than an acidic one are the Nb-OH sites.

Catalytic experiments revealed the need for predominantly acidic sites for succinic acid synthesis under CWO reaction conditions, while the FDCA synthesis requires catalysts with predominantly basic sites in nature and organic peroxides as oxidation agents.

## CHAPTER 6: Upgrade of 5-hydroxymethylfurfural to dicarboxylic acids onto multifunctional based $\text{Fe}_3\text{O}_4@/\text{SiO}_2$ magnetic catalysts

The main purpose of this study was to compare recoverable magnetic core supported noble (Ru) and transition (Mn, Co, Fe) metal oxide catalysts for HMF oxidation. The replacement of inorganic bases by amines and the direct functionalization of the catalysts with amines represented other aims in these reactions.

In the presence of Ru (4wt%)- $\text{Fe}_3\text{O}_4@/\text{SiO}_2$ , a selectivity to FDCA of 64% was reached after 48h for a total conversion of HMF (Figure 4A). The difference in the selectivity corresponded to MAc (15%) and to by-products resulted from MAc (i.e., tartaric acid (TarAc), MalAc and FumAc). The modification of the catalyst by *n*-butylamine led to a slight decrease in the HMF conversion to 92%, but to a substantial increase of the selectivity to FDCA to 80.6% (Figure 4B).

Whereas, the main results obtained in the HMF oxidation on  $\text{Fe}_3\text{O}_4@/\text{SiO}_2\text{-MnO}_x$  and  $\text{-CoO}_x$  catalysts are presented in Table 4. The Mn catalysts display low catalytic efficiency in the absence of a base. On the other hand, only high manganese concentrations (i.e., 10wt%) enabled the HMF transformation but with a low conversion (5%). Under these conditions the selectivity to MAc was of 72%, and to 5-hydroxymethyl-2-furancarboxylic acid (HMFCa) of 14.6% (Table 4, entry 1). In the presence of NaOH, the conversion of HMF increased until 100% but HMF was preponderantly transformed into humins. With this catalyst, the presence of weaker bases such as  $\text{Na}_2\text{CO}_3$  or *n*-butylamine had no beneficial effect on the oxidation of HMF.

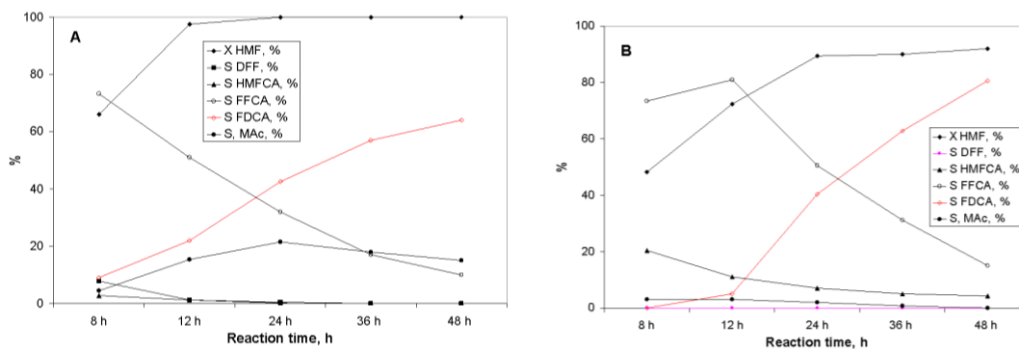


**Figure 4.** Time-evolution of the HMF oxidation in the presence of Ru (4wt%)- $\text{Fe}_3\text{O}_4@/\text{SiO}_2$  (catalytic sites: cationic ruthenium (III) docked onto  $-\text{NH}_2$  groups) (A) and *bis*-amine modified Ru (4wt%)- $\text{Fe}_3\text{O}_4@/\text{SiO}_2$  (B) catalysts (catalytic sites: Ru(IV)-*bis*-amine adducts).

**Table 4:** Catalytic oxidation of HMF in the presence of MnO<sub>x</sub>- and CoO<sub>x</sub>-Fe<sub>3</sub>O<sub>4</sub>@SiO<sub>2</sub> catalysts

| Entry           | Catalyst   | Additive                        | X, % | S <sub>HMFCa</sub> , % | S <sub>MAc</sub> , % | S <sub>SA</sub> , % |
|-----------------|--|---------------------------------|------|------------------------|----------------------|---------------------|
| 1               | Fe <sub>3</sub> O <sub>4</sub> @SiO <sub>2</sub> -MnO <sub>x</sub> (10%) | -                               | 5.0  | 14.6                   | 72.0                 | 0                   |
| 2 <sup>a</sup>  | Fe <sub>3</sub> O <sub>4</sub> @SiO <sub>2</sub> -MnO <sub>x</sub> (10%) | NaOH                            | 10.5 | 43.3                   | 0                    | 0                   |
| 3 <sup>b</sup>  | Fe <sub>3</sub> O <sub>4</sub> @SiO <sub>2</sub> -MnO <sub>x</sub> (10%) | NaOH                            | 100  | 9.5                    | 5.7<br>(malic acid)  | 19.3                |
| 4 <sup>c</sup>  | Fe <sub>3</sub> O <sub>4</sub> @SiO <sub>2</sub> -MnO <sub>x</sub> (10%) | Na <sub>2</sub> CO <sub>3</sub> | 4.4  | 100                    | 0                    | 0                   |
| 5 <sup>d</sup>  | Fe <sub>3</sub> O <sub>4</sub> @SiO <sub>2</sub> -MnO <sub>x</sub> (10%) | <i>n</i> -butylamine            | 10.6 | 10.6                   | 0                    | 1.8                 |
| 6               | Fe <sub>3</sub> O <sub>4</sub> @SiO <sub>2</sub> -CoO <sub>x</sub> (1%)  | -                               | 0    | 0                      | 0                    | 0                   |
| 7               | Fe <sub>3</sub> O <sub>4</sub> @SiO <sub>2</sub> -CoO <sub>x</sub> (5%)  | -                               | 20.3 | 33.3                   | 46.0                 | 0                   |
| 8               | Fe <sub>3</sub> O <sub>4</sub> @SiO <sub>2</sub> -CoO <sub>x</sub> (10%) | -                               | 100  | 0                      | 59.0                 | 10.0                |
| 9 <sup>a</sup>  | Fe <sub>3</sub> O <sub>4</sub> @SiO <sub>2</sub> -CoO <sub>x</sub> (10%) | NaOH                            | 78.6 | 3.3                    | 0                    | 92.7                |
| 10 <sup>b</sup> | Fe <sub>3</sub> O <sub>4</sub> @SiO <sub>2</sub> -CoO <sub>x</sub> (10%) | NaOH                            | 100  | 20.5                   | 0                    | 15.7                |
| 11              | Fe <sub>3</sub> O <sub>4</sub> @SiO <sub>2</sub> -CoO <sub>x</sub> (10%) | <i>n</i> -butylamine            | 97.7 | 22.6                   | 0                    | 11.4                |

**Reaction conditions:** 50 mg HMF (0.4 mmols), 25 mg catalyst, 5 mL H<sub>2</sub>O; 110°C, 10 bars O<sub>2</sub>, 8h; 9 mg *n*-butylamine (0.125 mmols); <sup>a</sup> - 0.39 mmol; <sup>b</sup> - 1.7 mmol; <sup>c</sup> - 0.39 mmol; <sup>d</sup> - 0.125 mmol

Recently, Hara et al. [27] reported the efficient HMF oxidation to FDCA (selectivity of 91%, for a total conversion of HMF) in the presence of MnO<sub>2</sub> and NaHCO<sub>3</sub>, at 10 atm O<sub>2</sub>, 100°C, after 24 h. These authors associated the catalysts performance to the oxidation state of manganese (MnO<sub>2</sub> > Mn<sub>2</sub>O<sub>3</sub> > Mn<sub>3</sub>O<sub>4</sub>). Also, various crystallographic phases of MnO<sub>2</sub> and particle size can significantly influence the catalytic behavior in this reaction. As demonstrated in the present work, the low crystallization of MnO<sub>2</sub> highly dispersed in the silica matrix favors the oxidative cleavage of C-C bond with formation of MAc, thus disfavoring the oxidation of HMF to FDCA.

In contrast to Mn-based catalysts, the Co-based catalysts provided high catalytic efficiency for the samples with lower loadings of Co. Thus, the 5wt% Co catalyst led to a conversion of 20.3% of HMF and a selectivity of 46% to MAc (Table 4, entry 7). Further increase of the loading to 10wt% led to a total conversion of HMF (Table 4, entry 8) with a selectivity to MAc of 59%.

High conversions of HMF (97.2%) with high selectivities to FDCA (68.6%) were recently reported using nano-Fe<sub>3</sub>O<sub>4</sub>-CoO<sub>x</sub> catalysts, *t*-BuOOH as oxidant, and DMSO as solvent. Co<sub>3</sub>O<sub>4</sub> and CoO were also reported as catalysts with moderate efficiency in the HMF oxidation (conversions of 16-40% and selectivities to FDCA smaller than 1%) [27]. However, the present work demonstrates that the addition of a base can dramatically change the performances of Fe<sub>3</sub>O<sub>4</sub>@SiO<sub>2</sub>-CoO<sub>x</sub>(10%) depending on the strength of the base. The presence of NaOH affords a conversion of HMF of 78.6% with selectivity to SA of 92.7% (Table 4, entry 9), while *n*-butylamine yields an even higher conversion (97.7%) leading to the selective production of HMFCa (Table 4, entry 11).

## Conclusions

In summary, Ru(IV)-bis-amine adducts afford an efficient catalytic system for the oxidation of HMF to FDCA. As we already demonstrated, the addition of *n*-butylamine changes the oxidation potential of the ruthenium species. This effect provides access to high selectivities to FDCA (80.6%) for a 92% conversion of HMF, as previously reported for the case of glucose CWO to SA.

Under similar conditions, replacing the noble metal with a transitional oxide tuned the selectivity in the sense of the production of other valuable products, such as MAc or SA. Accordingly, the Fe<sub>3</sub>O<sub>4</sub>@SiO<sub>2</sub>-CoO<sub>x</sub>(10wt%) catalyst provided a selectivity of 92.7% to SA for a HMF conversion of 78.6%, while for Fe<sub>3</sub>O<sub>4</sub>@SiO<sub>2</sub>-MnO<sub>x</sub>(10%) a selectivity of 72% to MAc was reached, but for a much smaller conversion of HMF(5%).

Interestingly, the functionalization of Fe<sub>3</sub>O<sub>4</sub>@SiO<sub>2</sub> with amino groups (Fe<sub>3</sub>O<sub>4</sub>@SiO<sub>2</sub>-NH<sub>2</sub>) enhanced the catalyst performance, providing selectivity to MAc of 85% for a HMF conversion of 35.6%. To our best knowledge, this is the highest selectivity to MAc reported to date for a heterogeneous catalyst.

The catalysts were magnetically separable, and showed no significant loss in catalytic activity during several recycling experiments.

## CHAPTER 7: Multifunctional nanocomposites with non-precious metals and magnetic core for 5-HMF oxidation to FDCA

The main purpose of the presented work in this chapter was to design and develop an efficient multi-functional magnetic nanocomposites catalytic system for the selective HMF oxidation to FDCA by combining Mn, Co and Fe oxides with NbMCM-41 as a shell of the MNP core. These materials combine unique oxidation properties with practical separation advantages.

Table 5 presents the main catalytic results using mono-functional catalysts and *t*-butyl hydroperoxyde (*t*-BOOH) as an oxygen transfer agent.

Table 5 shows mono-functional catalysts (i.e., xNb@MNP and MO<sub>x</sub>-SiO<sub>x</sub>@MNP) display from moderate to high HMF conversions (Table 5, entries 1-6). However, after 12 h of reaction no FDCA product was identified into the reaction products, irrespective of the catalyst, but only oxidation intermediates as HMFA and FFCA. For xNb@MNP samples the distribution of the reaction products was highly influenced by the loading of niobium: the higher the loading led to the higher selectivity to FFCA (Table 5, entries 1 and 2). The incorporation of Nb(V) in the MCM-41 structure generates an excess of positive charge in the framework (Nb<sup>+</sup> which plays the role of Lewis acid sites), balanced by Nb-O<sup>-</sup> sites (base sites) during dehydroxylation, as already Ziolek et al [28] demonstrated.

**Table 5:** The oxidation of HMF in the presence of mono-functional catalysts

| Entry          | Catalyst                                | C, % | S <sub>HMFA</sub> , % | S <sub>FFCA</sub> , % | S <sub>FDCA</sub> , % |
|----------------|---|------|-----------------------|-----------------------|-----------------------|
| 1              | 22Nb@MNP (Si/Nb = 22)                   | 80.8 | 0                     | 100                   | 0                     |
| 2              | 50Nb@MNP (Si/Nb = 50)                   | 85.2 | 90.7                  | 9.3                   | 0                     |
| 3              | CoO <sub>x</sub> -SiO <sub>2</sub> @MNP | 91.1 | 87.8                  | 12.1                  | 0                     |
| 4 <sup>a</sup> | CoO <sub>x</sub> -SiO <sub>2</sub> @MNP | 100  | 12.1                  | 72.0                  | 15.8                  |
| 5              | MnO <sub>x</sub> -SiO <sub>2</sub> @MNP | 88.1 | 75.7                  | 24.3                  | 0                     |
| 6 <sup>a</sup> | MnO <sub>x</sub> -SiO <sub>2</sub> @MNP | 100  | 0                     | 100                   | 0                     |
| 7              | FeO <sub>x</sub> -SiO <sub>2</sub> @MNP | 79.1 | 0                     | 100                   | 0                     |

**Reaction conditions:** HMF (0.2 mmoli; 25 mg); ACN 4.4 mL; 12h; 100 °C; 0.18 mL 70% *t*-BuOOH, 25 mg

However, even if mono-functional samples (22Nb@MNP and 50Nb@MNP) were active in the oxidation of HMF the presence of these species was not enough to run the oxidation of HMF to FDCA, and therefore the product mixture contained HMFA and FFCA intermediates (Table 5).

For MO<sub>x</sub>-SiO<sub>x</sub>@MNP samples, higher amounts of FFCA were produced by FeO<sub>x</sub>-SiO<sub>2</sub>@MNP (Table 5, entry 7). However, increasing the reaction time from 12 to 24h led to the diminution of FDCA, this being identified only with CoO<sub>x</sub>-SiO<sub>2</sub>@MNP (Table 5, entry 4). Also important, no DFF intermediate was evidenced irrespective of the catalytic active phase nature. However, the presence of Co<sup>2+</sup>/Co<sup>3+</sup> and Mn<sup>4+</sup>, as determined by XRD, seems to not favor the FDCA formation neither in catalytic wet oxidation conditions nor in the presence of an oxygen donor like *t*-BOOH, in this work.

Finally, mixing the two catalytic phases (i.e., Nb and a metal oxide) led to unexpected active and selective multifunctional materials. Thus, the 10M@xNb@MNP (where: M = Co, Mn or Fe) catalysts showed a higher catalytic efficiency for the selective oxidation of HMF to FDCA than any other catalytic system based on non-precious metals reported until now [29].

As Table 6 shows the most appropriate solvent for HMF oxidation to FDCA by *t*-BOOH is acetonitrile. In water a high amount of HMF is decomposed with the formation of glycolic acid (Table 6, entries 3 and 8), while in the water:methanol mixture (Table 6, entry 4) the oxidation stops to FDCA intermediates (i.e., HMFA and FFCA). No DFF intermediate was identified.

Irrespective of the MO<sub>x</sub> nature, an increased amount of Nb (from Si/Nb=50 to Si/Nb=22) led to increased selectivities to FDCA, although in different proportions (Table 6, entries: 1, 5, 6, 9, 10 and 12). For samples with Si/Nb=22, the selectivity to FDCA decreased in the order: Mn (76.6%) > Co (20.1%) > Fe (9.3%).

**Table 6:** The main results obtained in the oxidation of HMF in the presence of bifunctional catalysts

| Entry           | Catalyst,<br>@MNP | C, % | S <sub>HMFA</sub> , % | S <sub>FFCA</sub> , % | S <sub>FDCA</sub> , % |
|-----------------|-------------------|------|-----------------------|-----------------------|-----------------------|
| 1               | 10Co@22Nb         | 94.5 | 2.1                   | 77.8                  | 20.1                  |
| 2 <sup>a</sup>  | 10Co@22Nb         | 96.6 | 0.8                   | 2.7                   | 96.5                  |
| 3 <sup>b</sup>  | 10Co@22Nb         | 11.9 | 55.2                  | 0                     | 0                     |
| 4 <sup>c</sup>  | 10Co@22Nb         | 12.0 | 60.8                  | 39.2                  | 0                     |
| 5               | 10Co@50Nb         | 96.3 | 13.1                  | 86.2                  | 0.7                   |
| 6               | 10Mn@22Nb         | 97.7 | 2.5                   | 20.9                  | 76.6                  |
| 7 <sup>a</sup>  | 10Mn@22Nb         | 98.7 | 5.8                   | 7.25                  | 87.0                  |
| 8 <sup>b</sup>  | 10Mn@22Nb         | 36.6 | 63.8                  | 0                     | 0                     |
| 9               | 10Mn@50Nb         | 97.6 | 14.4                  | 83.9                  | 1.7                   |
| 10              | 10Fe@22Nb         | 96.7 | 69.8                  | 20.8                  | 9.3                   |
| 11 <sup>a</sup> | 10Fe@22Nb         | 99.7 | 3.03                  | 2.9                   | 94.1                  |
| 12              | 10Fe@50Nb         | 98.8 | 77.1                  | 16.6                  | 6.3                   |
| 13 <sup>a</sup> | 10Fe@50Nb         | 98.7 | 5.5                   | 29.6                  | 64.9                  |

**Reaction conditions:** HMF (0.2 mmoles; 25 mg); ACN 4.4 mL; 12h; 100 °C; 0.18 mL 70% *t*-BuOOH, 25 mg catalyst; <sup>a</sup> - 24h; <sup>b</sup> - water, 4.4 mL ; <sup>c</sup>-water:methanol (50:50 vol/vol), 4.4 mL. In water, the difference in selectivity till 100% corresponds to glycolic acid.

After 24h of reaction, the selectivity in FDCA was highly improved for the conversions of HMF higher than 96% (Table 6, entries: 2, 7 and 11). Accordingly, for the samples with

Si/Nb=22, the selectivity to FDCA increased to values of 87.0 - 96.5% decreasing in the following order: Co (96.5%) > Fe (94.1%) > Mn (87.0%). Lower loadings of Nb (i.e., Si/Nb = 50) exhibited a detrimental effect upon the selectivity to FDCA. Accordingly, it decreased from 94.1% (10Fe@22Nb@MNP) till 64.9% (10Fe@50Nb@MNP), while the conversion of HMF recorded an insignificant variation from 99.7% (10Fe@22Nb@MNP) to 98.7% (10Fe@50Nb@MNP) (Table 6, entries: 11 and 13).

The correlation between textural properties and selectivity to FDCA has been proven by corroboration the XRD and BET results. The high active samples, irrespective of the niobium loading or the nature of the MO<sub>x</sub> phase, showed a lack of the diffusion effects. As the adsorption-desorption isotherms of nitrogen at 77 K measurements showed, all samples display a disordered hexagonal pore packing with the simultaneous presence of internal pores and irregular secondary intercrystalline cavities, with sizes large enough to not impose restrictions to HMF diffusion. However, the textural properties correlate to the FDCA selectivity. The selectivity to FDCA follows the same tendency as the evolution of the surface area and the pore volume of the catalysts. Both decrease in the same order: Co > Fe > Mn. In conclusion, the higher the surface area and the pore volume, the higher was the selectivity to FDCA.

In the presence of the bi-functional catalysts the DFF intermediate was not identified, irrespective of the solvent nature. Therefore, the reasonable reaction pathway of the HMF oxidation over 10M@xNb@MNP should follow the HMF → HMFCa → FFCA → FDCA route.

## Conclusions

In summary, 10M@xNb@MNP bifunctional catalysts afford unexpected highly efficient catalytic systems for the oxidation of HMF to FDCA. In our best knowledge, this is the first time when a catalytic system based on transitional metals follows a characteristic mechanism for noble metals, taking place through the adsorption of an aldehyde C-HO group through a HMF → HMFCa → FFCA → FDCA sequence. The advantage of this new bifunctional system over the use of noble metals is that such a mechanism does not claim the presence of a homogeneous base.

The obtained results support a concerted effect of both textural and structural characteristics of the catalysts upon the produced FDCA selectivity. The magnitude of the FDCA selectivity follows the surface areas and the pore volumes decreasing in the same order: Co > Fe > Mn. In other words, a higher surface area and pore volume correspond to a higher selectivity to FDCA. Moreover, combining MO<sub>x</sub> (CoO<sub>x</sub>, MnO<sub>x</sub> or FeO<sub>x</sub>) with niobium species generate a synergetic effect in which MO<sub>x</sub> acts as a co-catalyst for niobium sites by furnishing the hydroxyl species through the *t*-BuOOH decomposition. Once formed these hydroxyl groups are catch by the Nb<sup>+</sup> species generating the active sites for the dehydrogenation of oxidated intermediates to FDCA. Following this pathway the 10Co@22Nb@MNP catalyst is able to produce FDCA with a selectivity of 96.5%, for a HMF conversion of 96.6%, while 10Fe@22Nb@MNP led to a selectivity of 94.1% to FDCA for a HMF conversion of 99.7%. The catalysts were magnetically separable, and showed no significant loss in the catalytic activity during several recycling experiments.

## CHAPTER 8: From useless humins by-product to Nb@graphite-like carbon catalysts highly efficient in HMF synthesis

In this chapter humins by-products obtained from dehydration of glucose were employed as carrier to prepare a novel niobium-based carbonaceous solid catalyst. The catalysts preparation methodology induces structural modifications of the humin carrier with the formation of a highly hydrophobic graphite-like carbon structure and generation of acid-base functionalities. The catalytic performances of the humin-derived Nb-based catalysts were investigated in the direct dehydration reaction of D-glucose to HMF.

In this study, the catalytic behavior of the niobia/humins catalysts was investigated in the one-pot conversion of the glucose to HMF in a biphasic system consisting of a combination of glucose dehydration under aqueous conditions and an *in situ* extraction of the HMF in an organic phase [23]. With this purpose, different phases as methyl-isobutyl-ketone (MIBK), 2-tert-butylphenol (TBP) and 2-sec-butylphenol (SBP) were used as an extraction solvent. Previously work conducted in our group, showed that highly dispersed Nb species into a zeolite matrix [30] display a high catalytic efficiency in glucose dehydration to HMF (selectivities to MHF of 84.3%, for a conversion of glucose of 97.4%, at 180°C and after 12h) in a biphasic water/MIBK solvent [23]. However, other reports indicate 2-sec-butylphenol (SBP) as an efficient extraction solvent, its advantage being generate by high HMF yields compared to other organic solvents such as tetrahydrofuran (THF), methyl isobutyl ketone (MIBK), and 2-butanol [31].

In this study, the results collected from a series of catalytic experiments highlighted some very important features. Reactions carried out at 140-180°C for 6-12h led to very good yield to HMF, with a maximum for a temperature of 180°C and a reaction time of 8h, irrespective of the extracting solvent (i.e., MIBK, TBP and SBP) or the catalyst nature. However, the presence of NaCl in the aqueous phase induces an important difference between an inefficient and a highly efficient catalytic system (Table 7).

As Table 7 shows, in the presence of the calcined humins no HMF was detected into reaction products (Table 7, entry 1,) that might be attributed to the graphite-like carbon structure of calcined humins with a low concentration of weak surface acid/base functional groups. The HMF production in pure water or TBP, as monophasic solvent, is also not a viable option for the HMF synthesis (GHNb1.2 catalyst, in monophasic solvent, Table 7, entry 2 and 3,), presumably due to the slow rate of HMF formation and fast rehydration to furan ring opening products, such as levulinic acid (LA) and formic acid.

**Table 7.** Catalytic results in glucose dehydration to HMF in biphasic systems

| Entry          | Catalyst    | Solvent    | Yield HMF, (%) |
|----------------|-------------|------------|----------------|
| 1              | Calcined GH | TBP/water  | 0              |
| 2              | GHNb1.2     | Water      | 0              |
| 3              | GHNb1.2     | TBP        | 0              |
| 4 <sup>a</sup> | GHNb1.2     | TBP/water  | 16             |
| 5              | GHNb1.2     | TBP/water  | 96             |
| 6              | GHNb1.2     | SBP/water  | 38             |
| 7              | GHNb1.2     | MIBK/water | 15             |
| 8              | GHNb1.7     | TBP/water  | 85             |
| 9              | GHNb1.7     | SBP/water  | 24             |
| 10             | GHNb1.7     | MIBK/water | 14             |

*Reaction conditions:* glucose 0.18g (1mmol), 50mg of catalyst, solvent [3.5ml H<sub>2</sub>O (NaCl 20%) + 1.5ml

---

extracting solvent], reaction temperature: 180°C, reaction time: 8h, 1000 rpm;

<sup>a</sup> - no NaCl in aqueous phase

As Table 7 shows, in the presence of the calcined humins no HMF was detected into reaction products (Table 7, entry 1,) that might be attributed to the graphite-like carbon structure of calcined humins with a low concentration of weak surface acid/base functional groups. The HMF production in pure water or TBP, as monophasic solvent, is also not a viable option for the HMF synthesis (GHNb1.2 catalyst, in monophasic solvent, Table 7, entry 2 and 3,), presumably due to the slow rate of HMF formation and fast rehydration to furan ring opening products, such as levulinic acid (LA) and formic acid.

Replacing the monophasic solvent with a bi-phasic TBP/water, the HMF starts to accumulate (Table 7, entry 4) and a yield of 16% HMF was determined in reaction products. However, as already reported [32], the presence of NaCl in the aqueous phase plays an important role in improving the partition coefficient of HMF. Indeed, in bi-phasic TBP/water system and 20%NaCl in the aqueous phase, the yield to HMF highly increased from 16% to 96% (Table 7, entry 5).

The nature of the catalysts and organic solvents plays an important role in determining an effective extraction of HMF. Using the same approach, i.e. a biphasic system consisting of methyl-isobutyl-ketone (MIBK) as extraction solvent and aqueous NaCl (20%) salt, Nb-based humins catalysts produced HMF in much lower yields (15%, on GHNb1.2 catalyst) than previously reported Nb-based Beta zeolite catalysts (82.1% at 180°C and 12 h). Moreover, these catalysts have different degrees of hydrophilicity. Accordingly, the Nb-based Beta zeolite catalyst was located in the aqueous phase while the GHNb1.2 one was located in the organic phase indicating its high hydrophobicity. Such a behavior led to significant differences in the glucose conversion to HMF. This statement is also supported by the work of Datye and co-workers [33] which showed that different applied preparation methodologies lead to Nb-based carbonous carriers with different degrees of hydrophilicity, and hence with different locations in the biphasic water/SBP system. According with this location their catalytic behavior in the conversion of glucose to HMF was highly affected. A comparison of the obtained results in this work with those reported by Datye and co-workers [33], in similar biphasic systems, indicates the superiority of our developed materials in terms of HMF yields. Clearly enough, the differences highly depend on both the location of the catalyst and the intrinsic catalytic features.

However, by changing the extraction solvent from MIBK to SBP, in the presence of GHNb1.2 catalyst and under similar reaction conditions, the yield in HMF increased to 57%, after only 8h (Table 7, entry 6). The different reaction results are supported by the value of the partition coefficient which highly increases for all organic solvents in the presence of NaCl. Its relative increases depends on the nature of the organic solvent and is explained by a salting-out effect [34].

Working under the same experimental conditions in the presence of the GHNb1.7 the trend was similar but the yields were smaller than those obtained in the presence of the GHNb1.2 (Table 7, entries 8-10). With GHNb1.7 the highest yield to HMF (85%) was obtained in bi-phasic TBP/water and 20%NaCl in the aqueous phase, while in bi-phasic SBP/water system and 20%NaCl in the aqueous phase, the yield to HMF reached only 24%. These results confirm the importance of the basic/acid ratio in this reaction. As XPS measurements showed, the concentration of superficial niobium is similar in both GHNb1.2 and GHNb1.7 catalysts but the TPD measurements evidenced a much higher basic/acid sites ratio in the GHNb1.7 one (4.25). However, GHNb1.7 led to lower yields to HMF. A high yield to HMF requires an optimum

base/acid sites ratio and as it has been demonstrated this condition is fulfilled for GHNb1.2 with a ratio of 1.76.

## Conclusion

In summary, in this paper we report a novel active and selective catalyst for the one-pot catalytic transformation of glucose to HMF, prepared by the deposition precipitation-carbonization (DPC) of ammonium niobate(V) oxalate hydrate over humins carrier produced by glucose dehydration. After calcination resulted catalysts with highly dispersed niobia particles anchored onto the graphite-like carbon carrier. This preparation procedure afforded an unexpected highly efficient catalyst for the HMF synthesis. The distribution of niobium species on the carrier surface makes the difference between an efficient and an less-efficient catalyst. Thus, for the same concentration of surface niobium (i.e., 2.4at% from XPS analysis) deposited on, a relatively more homogeneous distribution (SEM analysis) as -Nb-OH and Nb=O species (DRIFT analysis) leads to an efficient catalyst while the agglomeration in relatively rich areas determines an appreciable decrease of the HMF yield. The relative base/acid sites ratio is influenced by the distribution of niobium and the formation of Nb-rich particles.

The highest yield to HMF (96%) was obtained with the GHNb1.2 (0.03moles% Nb) catalyst in a bi-phasic TBP/water system, at 180°C after 8h.

In conclusion, these results confirm that by-products of renewable biomass-based technologies, such as humins, may offer valuable solutions for the production of important chemicals, such as HMF and, in this way, for the utilization of an effective this approach concerned to the circular economy concept support for a sustainable economy.

## Selected references

- [1] B. M. Stadler, A. Brandt, A. Kux, H. Beck and J. G. d. Vries. Properties of novel polyesters made from renewable 1,4-pentanediol. *ChemSusChem*. 13 (2020) 556–563
- [2] X. Wu, N. Luo, S. Xie, H. Zhang, Q. Zhang, F. Wang and Y. Wang. Photocatalytic transformations of lignocellulosic biomass into chemicals. *Chem. Soc. Rev.* 49 (2020) 6198–6223
- [3] A. Wang and T. Zhang. One-Pot Conversion of Cellulose to Ethylene Glycol with Multifunctional Tungsten-Based Catalysts. *Acc. Chem. Res.*, 7 (2013) 1377–1386
- [4] A. Shrotri, H. Kobayashi, and A. Fukuoka. Cellulose Depolymerization over Heterogeneous Catalysts. *Acc. Chem. Res.*, 51 (2018) 761–768
- [5] S. Takkellapati, T. Li and M. A. Gonzalez. An overview of biorefinery-derived platform chemicals from a cellulose and hemicellulose biorefinery. *Clean Techn. Environ. Policy*. 20 (2018) 1615–1630
- [6] H. Choudhary, S. Nishimura and K. Ebitani. Metal-free oxidative synthesis of succinic acid from biomass-derived furan compounds using a solid acid catalyst with hydrogen peroxide. *Applied Catalysis A: General*. 458 (2013) 55–62
- [7] L. Xue, K. Chenga, H. Zhang, W. Denga, Q. Zhanga, and Y. Wang. Mesoporous H-ZSM-5 as an efficient catalyst for conversions of cellulose and cellobiose into methyl glucosides in methanol. *Catal. today*, 274 (2016) 60–66
- [8] S. M. Csicsery. *Catalysis by shape selective zeolites — science and technology* P.O.Box 843, Lafayette, California, 94549 USA (1995)
- [9] A. Corma, F. X. L. Xamena, C. Prestipino, M. Renz and S. Valencia. Water Resistant, Catalytically Active Nb and Ta Isolated Lewis Acid Sites, Homogeneously Distributed by Direct Synthesis in a Beta Zeolite. *J. Phys. Chem.C*, 113 (2009) 11306–11315
- [10] B. Liu and Z. Zhang. Catalytic Conversion of Biomass into Chemicals and Fuels over Magnetic Catalysts. *ACS Catal.* 6 (2016) 326–338

- [11] H. Kim, S. Lee, B. Lee, J. Park, H. Lim and W. Won. Improving revenue from lignocellulosic biofuels: An integrated strategy for coproducing liquid transportation fuels and high value-added chemicals. *Fuel*. 287 (2021) 119369
- [12] S. Sukanuma, K. Nakajima, M. Kitano, D. Yamaguchi, H. Kato, S. Hayashi and M. Hara. Hydrolysis of cellulose by amorphous carbon bearing SO<sub>3</sub>H, COOH, and OH groups. *J. Am. Chem. Soc.* 130 (2008)12787–12793
- [13] Radarweg 29, PO Box 211, 1000 AE Amsterdam, The Netherlands The Boulevard, Langford Lane, Kidlington, Oxford, OX5 1GB, UK 1st edition (2013)
- [14] J. C. Védrine. Heterogeneous Catalysis on Metal Oxides. *Catalysts*, 7 (2017) 341
- [15] M. V. Twigg, “Catalyst Handbook Mansson,” 2nd Edition, Manson Publishing, London, (1994)
- [16] M. Thommes, K. Kaneko, A. V. Neimark, J. P. Olivier, F. R. Reinoso, J. Rouquerol and K. S. W Sing. Physisorption of Gases, with Special Reference to the Evaluation of Surface Area and Pore Size Distribution (IUPAC Technical Report). *Pure Appl. Chem.* 87 (2015) 1051–1069
- [17] I. Podolean, V. Kuncser, N. Gheorghe, D. Macovei, V. I. Parvulescu and S. M. Coman. Ru-based magnetic nanoparticles (MNP) for succinic acid synthesis from levulinic acid. *Green Chem.* 15 (2013) 3077–3082
- [18] S. M. Coman, G. Pop, C. Stere, V. I. Parvulescu, J. El Haskouri, D. Beltrán and P. Amorós. New heterogeneous catalysts for greener routes in the synthesis of fine chemicals, *J. Catal.*, 251 (2007) 388–399
- [19] S. M. Coman, M. Verziu, A. Tirsoaga, B. Jurca, C. Teodorescu, V. Kuncser, V. I. Parvulescu, G. Scholz and E. Kemnitz. NbF<sub>5</sub>–AlF<sub>3</sub> Catalysts: Design, Synthesis, and Application in Lactic Acid Synthesis from Cellulose. *ACS Catal.* 5 (2015) 3013–3026
- [20] K. Shimizu, R. Uozumi and A. Satsuma. Enhanced production of hydroxymethylfurfural from fructose with solid acid catalysts by simple water removal methods. *Catal. Commun.* 10 (2009) 1849–1853
- [21] A. Herbst and C. Janiak. Selective glucose conversion to 5-hydroxymethylfurfural (5-HMF) instead of levulinic acid with MIL-101Cr MOF-derivatives. *New J. Chem.* 40 (2016) 7958–7967
- [22] F. Tielens, T. Shishido and S. Dzwigaj. What Do the Niobium Framework Sites Look Like in Redox Zeolites? A Combined Theoretical and Experimental Investigation, *J. Phys. Chem. C.* 114 (2010) 3140–3147
- [23] N. Candu, M. E. Fergani, M. Verziu, B. Cojocar, B. Jurca, N. Apostol, C. Teodorescu, V. I. Parvulescu and S. M. Coman. Efficient glucose dehydration to HMF onto Nb-BEA catalysts, *Catal. Today*, 325 (2019) 109–116
- [24] D. Lei, K. Yu, M. R. Li, Y. L. Wang, Q. Wang, T. Liu, P. K. Liu, L. L. Lou, G. C. Wang and S. X. Liu. Facet Effect of Single-Crystalline Pd Nanocrystals for Aerobic Oxidation of 5-Hydroxymethyl-2-furfural, *ACS Catal.* 7 (2017) 421–432
- [25] A. Tirsoaga, M. E. Fergani, N. Nuns, P. Simon, P. Granger, V. I. Parvulescu and S. M. Coman. Multifunctional nanocomposites with non-precious metals and magnetic core for 5-HMF oxidation to FDCA. *Appl. Catal. B: Environ.* 278 (2020) 119309
- [26] B. Donoeva, N. Masoud and P. E. D. Jongh. Carbon Support Surface Effects in the Gold-Catalyzed Oxidation of 5-Hydroxymethylfurfural, *ACS Catal.* 7 (2017) 4581–4591
- [27] E. Hayashi, T. Komanoya, K. Kamata and M. Hara. Heterogeneously-catalyzed Aerobic Oxidation of 5-Hydroxymethylfurfural to 2,5-Furandicarboxylic Acid with Manganese Dioxide. *ChemSusChem.* 10 (2017) 654–658
- [28] M. Ziolk, I. Nowak, I. Sobczak, A. Lewandowska, P. Decyk and J. Kujawa. Physico-chemical and catalytic properties of MCM-41 mesoporous molecular sieves containing transition metals (Cu, Ni, and Nb). *Stud. Surf. Sci. Catal.* 129 (2000) 813–822
- [29] P. Pal and S. Saravanamurugan. Recent Advances in the Development of 5- Hydroxymethylfurfural Oxidation with Base (Nonprecious)- Metal- Containing Catalysts. *ChemSusChem.* 10 (2019) 145–163
- [30] M. E. Fergani, N. Candu, S. M. Coman and V. I. Parvulescu. Nb-Based Zeolites: Efficient bi-Functional Catalysts for the One-Pot Synthesis of Succinic Acid from Glucose. *Molecules.* 22(12) (2017) 2218
- [31] Y. J. P. Torres, T. Wang, J. M. R. Gallo, B.H. Shanks and J. A. Dumesic. Production of 5-Hydroxymethylfurfural from Glucose Using a Combination of Lewis and Brønsted Acid Catalysts in Water in a Biphasic Reactor with an Alkylphenol Solvent. *ACS Catal.* 2 (2012) 930–934
- [32] B. Saha and M. M. A. Omar. Advances in 5-Hydroxymethylfurfural Production from Biomass in Biphasic Solvents. *Green Chem.* 16 (2014) 24–38
- [33] H. Xiong, T. Wang, B. H. Shanks and A. K. Datye. Tuning the Location of Niobia/Carbon Composites in a Biphasic Reaction: Dehydration of D-Glucose to 5-Hydroxymethylfurfural. *Catal. Lett.* 143 (2013) 509–516
- [34] T. C. Tan and S. Aravindh. Liquid–liquid equilibria of waterracetic acid/1-butanol system —effects of sodium potassium chloride and correlations. *Fluid Phase Equilib.* 163 (1999) 243–257

## General Conclusions

Utilization of the biomass for the production of chemical compounds and biofuels became an essential strategy to achieve a more sustainable and green economy. In this context, the conversion of lignocellulosic biomass has become one of the most widely studied processes because of several advantages. Thus, it is based on the valorization of the use of inedible and inexpensive carbon neutral. Such a biomass is also one of the most abundant containing carbon renewable feedstocks on the earth.

Based on this new strategy it is clearly the urgency to develop novel catalytic systems able to afford high conversions and selectivities of these valuable renewable feedstocks with high reaction rates and selectivities. The use of the catalysts is therefore compulsory to achieve these goals; this strategy has to avoid noble metals. Their high price associated to the scarce disposal demands innovating cheap alternatives, where less expensive and more abundant transition metal-based heterogeneous catalysts would be preferred.

In line with this, the first and the second chapters provide a large analysis of the catalytic systems which could be utilized for the synthesis of valuable platform molecules such as: HMF, FDCA and SA. Based on a critical evaluation of this state of the art the main objective of this thesis was to develop an efficient and cheaper transition metal-catalyst deposited on different types of supports like zeolites, magnetic nanoparticles or humins.

*Chapter 1* discusses the recent advancement in the sustainability concept by considering the utilization of renewable raw materials. The specific properties of the various biomass feedstocks are associated/correlated to the requirements imposed to the new types of solids that have to be used as catalysts. It is also discussed the importance of investigated transformations of various lignocellulosic materials to bio-chemical molecules (such as HMF, MA, SA and FDCA), and important building blocks for the industrial chemistry.

*Chapter 2* analysis the development of green catalytic processes using heterogeneous catalytic systems. In this context, were analyzed different types of supports, such as zeolites, magnetic nanoparticles and humins, and the associated of these with nanoparticle metal oxides, such as  $\text{CoO}_x$ ,  $\text{MnO}_x$  and  $\text{NbO}_x$ . A comparison with the bulk oxides is also presented.

*Chapter 3* presents all the experimental steps (i.e., chemical reagents, methods and the practical procedures), considered for the preparation of the catalytic samples and the analysis procedure of the reaction products. There are also presented the characterization techniques utilized for an exhaustive characterization of the prepared catalysts (i.e., BET,  $\text{CO}_2/\text{NH}_3$ -TPD measurements, XRD, XPS, SEM-EDX, ToF-SIMS, ICP-OES, DLS, TG-DTA and DRIFT spectroscopy).

*Chapters 4 and 5* discuss Nb-based zeolites as highly efficient catalytic systems for the oxidation of glucose/HMF to SA or HMF to FDCA. Catalytic experiments revealed the need for predominantly acidic sites for succinic acid synthesis under CWO reaction conditions, while the FDCA synthesis requires catalysts with predominantly basic sites in nature and organic peroxides as oxidation agents. In the same time, the presence of mesopores into the catalysts structure may be of help for the reactants and products diffusion, which may be the reason for the high catalytic activity.

The characterization results showed that the geometry of Nb clearly depends on the synthesis method. Through the post-synthetic insertion of Nb (dealumination followed by Nb insertion) resulted Nb-zeolite series possessing a mono-modal mesoporous texture comprised from extra-framework isolated Nb(V) sites (corresponding to Nb(V)O-H species) and  $\text{Nb}_2\text{O}_5$

pore-encapsulated clusters (i.e., Nb-Y5, Nb-ZSM25, Nb-Y30, Nb- $\beta$ 12 and Nb- $\beta$ 18). Residual framework Al-acid sites are also formed, which prevent the solubilization of the zeolite framework in hot water, but also different amounts of extra framework  $\text{AlO}_x(\text{OH})$  species. Whereas, the direct synthesis procedure (i.e., Nb-Sil-1) led to a bi-modal micro-mesoporous structure with tetrahedral niobium species presenting  $-\text{Nb}=\text{O}$  group. The  $\text{CO}_2$ - and  $\text{NH}_3$ -TPD measurements evidenced the presence of both acid and basic sites and the only sites which may display a base character rather than an acidic one are the Nb-OH sites.

From the investigated Nb@Beta zeolites series the most significant performances were collected for the Nb(0.05)- $\beta$ -37.5 catalyst. With this catalyst the SA was directly produced from glucose in water, as solvent, and with molecular oxygen, as a sole oxidant, with a selectivity of 84%, for a total conversion of glucose, after 12h, at 180°C and 18 bars of oxygen. For FDCA the best catalytic results were obtained after 24–48 h, in the presence of Nb-ZSM25 (61.3% FDCA selectivity for a HMF conversion of 96.7%) and Nb-Si-1 (63.8% FDCA selectivity for a HMF conversion of 99.0%) catalysts, at 140°C, ACN as solvent and *t*-BuOOH as oxidant. The catalysts were recycled with no significant loss in the catalytic activity during several experimental steps.

The synthesis, catalytic behaviour and characterization of the  $\text{Fe}_3\text{O}_4@\text{SiO}_2$  core-shell carriers (i.e.,  $\text{Nb}_2\text{O}_5$ ,  $\text{CoO}_x$ ,  $\text{MnO}_x$  and  $\text{FeO}_x - \text{Fe}_3\text{O}_4$ ) as active catalysts was considered as an alternative to the high cost noble-metals based catalysts (*Chapters 6 and 7*):

The characterization of the catalysts indicated that the incorporated metal oxides ( $\text{MnO}_x$  and  $\text{CoO}_x$ ) were homogeneously highly dispersed on the  $\text{Fe}_3\text{O}_4@\text{SiO}_2$  core-shell. In the FTIR spectra the strong absorption band at  $1100\text{ cm}^{-1}$ , characteristic of the asymmetric stretching vibration of Si-O-Si bond, is shifted to  $1079\text{ cm}^{-1}$ , usually associated with the asymmetric stretching vibration of Si-O-M (M = Mn and Co, in these cases). For the  $\text{Fe}_3\text{O}_4@\text{SiO}_2\text{-MO}_x(10\text{wt}\%)$  series, the best results were obtained for  $\text{Fe}_3\text{O}_4@\text{SiO}_2\text{-CoO}_x(10\text{wt}\%)$  which provided a selectivity of 92.7% to SA for a HMF conversion of 78.6%. Under similar reaction conditions  $\text{Fe}_3\text{O}_4@\text{SiO}_2\text{-MnO}_x(10\text{wt}\%)$  provided a selectivity of 72% to MAc, but for a much smaller conversion of HMF (5%). The functionalization of  $\text{Fe}_3\text{O}_4@\text{SiO}_2$  with amino groups ( $\text{Fe}_3\text{O}_4@\text{SiO}_2\text{-NH}_2$ ) made possible the synthesis of MAc with a selectivity of 85% for a HMF conversion of 35.6%. To our best knowledge, this is the highest selectivity to MAc reported to date for a heterogeneous catalyst.

Mono- and multi-functional magnetic nanocomposites catalytic systems, based on Nb (i.e.,  $\text{Fe}_3\text{O}_4@\text{Si}/\text{Nb-MnO}_x$  and  $\text{Fe}_3\text{O}_4@\text{Si}/\text{Nb-CoO}_x$  catalysts) were investigated for the oxidation of HMF to FDCA in acetonitrile. In our best knowledge, this is the first time when a catalytic system based on transitional metals follows a characteristic mechanism for noble metals, taking place through the adsorption of an aldehyde C-HO group through a  $\text{HMF} \rightarrow \text{HMFCa} \rightarrow \text{FFCA} \rightarrow \text{FDCA}$  sequence. The characterization of the catalysts indicated that the magnitude of the FDCA selectivity follows the surface areas while the pore volumes decreased in the same order:  $\text{Co} > \text{Fe} > \text{Mn}$ . In other words, a higher surface area and pore volume corresponded to a higher selectivity to FDCA. Moreover, combining  $\text{MO}_x$  ( $\text{CoO}_x$ ,  $\text{MnO}_x$  or  $\text{FeO}_x$ ) with niobium species generate a synergetic effect in which  $\text{MO}_x$  acts as a co-catalyst for niobium sites by furnishing the hydroxyl species through the *t*-BuOOH decomposition. Once formed, these hydroxyl groups are catch by the  $\text{Nb}^+$  species generating the active sites for the dehydrogenation of oxidated intermediates to FDCA. The  $10\text{Co}@22\text{Nb}@\text{MNP}$  catalyst is able to produce FDCA with a selectivity of 96.5%, for a HMF conversion of 96.6%, while  $10\text{Fe}@22\text{Nb}@\text{MNP}$  led to a selectivity of 94.1% to

FDCA for a HMF conversion of 99.7%. The catalysts were magnetically separable and showed no significant loss in the catalytic activity during several recycling experiments.

The last chapter (**Chapter 8**) proposes novel catalytic materials which were developed using residual humins (by-products formed into the dehydration of glucose to HMF) as carriers and niobia, as catalytic active phase. This approach gave a positive economic and environmental impact, contributing to a cleaner production, in line to the concept of a circular economy. The characterization of the calcined catalysts shows that for the same concentration of surface niobium (i.e., 2.4at% from XPS analysis) deposited on, a relatively more homogeneous distribution (SEM analysis) as -Nb-OH and Nb=O species (DRIFT analysis) leads to an efficient catalyst, while the agglomeration in relatively rich areas determines an appreciable decrease of the HMF yield. Also, the relative base/acid sites ratio is influenced by the distribution of niobium, the formation of Nb-rich particles corresponding to an increased ratio. The catalyst GHNb1.2 exhibited excellent catalytic ability and efficiency for dehydration of glucose to HMF with a 96% yield, under the following reaction conditions: 3.5ml H<sub>2</sub>O [(NaCl 20%)]/1.5ml TBP, 180°C, 1000 rpm, for 8h.

Very important too, all developed catalysts are resistant under harsh reaction conditions. Moreover, these catalysts are easily separated and recycled several times.

In conclusion, the obtained results on the novel catalytic systems confirm a complete accomplishment of the objectives of this thesis. They give also a motivation for a further investigation/development of this topic in the bio-based industry.

## DISSEMINATION

The results of the PhD thesis were already disseminated in five scientific papers: **Molecules**, 22, 2218, **2017** (IF = **3.09**), **ACS Sustain. Chem. Eng.**, 6(11), 14292-14301, **2018** (IF = **7.63**), **Molecules**, 25, 4885, **2020** (IF = **3.26**), **Appl. Catal. B-Environ.** 278, 119309, **2020** (IF = **16.68**) and **Appl. Catal. A-Gen.** 618, 118130, **2021** (IF = **5.00**), with a cumulative impact factor of **35.66**. In addition, a number of **nine** presentations at international and national conferences, as **seven** oral presentations and **two** posters, have been also delivered.

*All these achievements are listed below.*

### List of publications relevant for the PhD thesis:

1. M. El Fergani, N. Candu, S. M. Coman and V. I. Parvulescu, Nb-based zeolites: efficient bi-functional catalysts for the one-pot synthesis of succinic acid from glucose. *Molecules*, 22 (2017) 2218 (IF = **3.09**).
2. A. Tirsoaga,\* M. El Fergani,\* V. I. Parvulescu and S. M. Coman, HMF upgrade to dicarboxylic acids on multifunctional based Fe<sub>3</sub>O<sub>4</sub>@SiO<sub>2</sub> magnetic catalysts. *ACS Sustain. Chem. Eng.*, 6(11) (2018) 14292-14301 (IF = **7.63**), \*- The authors has equal contribution.
3. M. El Fergani, N. Candu, M. Tudorache, P. Granger, S. M. Coman, and V. I. Parvulescu, Optimized Nb-Based Zeolites as Catalysts for the Synthesis of Succinic Acid and FDCA. *Molecules*, 25 (2020) 4885 (IF = **3.26**).
4. A. Tirsoaga, M. El Fergani, N. Nuns, P. Simon, P. Granger, V. I. Parvulescu and S. M. Coman, Multifunctional nanocomposites with non-precious metals and magnetic core for 5-HMF oxidation to FDCA. *Appl. Catal. B-Environ.* 278 (2020) 119309 (IF = **16.68**).

5. M. El Fergani, N. Candu, M. Tudorache, C. Bucur, P. Granger, S. M. Coman, From useless humin by-product to Nb@humin catalysts highly efficient in HMF synthesis. Appl. Catal. A-Gen. 618 (2021)118130 (**IF = 5.00**).

**Miscellaneous publications:**

1. M. Rahuma, H. Amir and M. El Fergani, Corrosion inhibition of mild Steel in 11% hydrochloric Acid Solutions by using Black pepper, Chem. Sci. Trans., 3 (2) (2014) 764-772 (**IF = 0.98**)
2. N. Candu, M. El Fergani, M. Verziu, B. Cojocaru, B. Jurca, N. Apostol, C. Teodorescu, V. I. Parvulescu and S. M. Coman, Efficient glucose dehydration to HMF onto Nb-BEA catalysts. Catal. Today. 325 (2019) 109-116 (**IF = 4.95**).